Supporting Information for

Cost and performance targets for fully electrochemical ammonia production under flexible operation

Nikifar Lazouski,[1] Aditya Limaye,[1] Abhishek Bose,[2] Michal L. Gala,[1] Karthish Manthiram,[3†] and Dharik S. Mallapragada,[2*]

[1]Department of Chemical Engineering; Massachusetts Institute of Technology; Cambridge, MA 02139, USA.

[2]MIT Energy Initiative, Massachusetts Institute of Technology; Cambridge, MA 02139, USA.

[3]Division of Chemistry and Chemical Engineering, California Institute of Technology, Pasadena, CA 91125, USA

[*]Correspondence to: dharik@mit.edu

[†]Correspondence to: karthish@caltech.edu

Supplementary Methods

Model details

The target plant ammonia discharge rate is set at 250 tons day^{-1}, which can be met through a combination of ammonia synthesis or discharge from on-site storage. This specific scale was chosen to balance the power consumption of a small-scale renewable energy farm (~50 MW) and economies of scale for costing and sizing components. However, it is worth mentioning that since most of the portions of the plant have cost curves that are linear in the production volume (e.g. electrochemical reactor stacks), the cost of ammonia is not expected to change significantly upon scaling the system as long as the technology and relative costs for various parts of the plant remain constant.

The only source of energy in the plant is assumed to be installed variable renewable electricity (VRE) generation, namely wind and photovoltaic (PV) installations. The power output, or capacity factor (CF) of installed generation is assumed to change hourly based on historical weather data. Hourly capacity factors for PV were obtained using the PVLIB model,[37] with historical satellite-derived weather data from the National Solar Radiation Database (NSRDB) used as inputs.[38] Wind power outputs are simulated using historical meteorological data from the NREL Wind Integration National Dataset Toolkit (WTK)[39] and using a commercial Gamesa G26/2500 turbine power curve data from wind turbines assuming a 100 hub height. Further details on VRE resource characterization are provided elsewhere.[28,40] Solar and wind capacity factors from 2011 were used for this study, as the weather patterns in that year were more representative of the average.

Table S1. System and electrochemical reactor parameter values used in the base case for the model and the ranges of values examined in the present analysis.

Parameter	Base value	Tested range
Maximum current density	500 mA cm^{-2}	100-2500 mA cm^{-2}
NH_3 Faradaic efficiency (FE)	70%	30-95%
Minimum NH_3 production rate at 100% FE	50 kmol/hr	0-1600 kmol/hr
Cell overpotential (at 10 mA cm^{-2})	0.8 V	0.2-3.8 V
Electrolyte resistivity	0.1 Ohm cm^2	0.1-10 Ohm cm^2
Reactor pressure	10 bar	2-30 bar
Reactor temperature	30 °C	30-90 °C

Table S2. Plant wide assumptions used for costs and productivity. References for parameter values are in parameter name superscripts; references to Supplemental Information (SI) include a derivation of the value in the Supplemental Information. An additional contingency factor of 21% is included in the model for all unit investment cost terms in the objective function.

Parameter	**Value**
Water electrolyzer cost[41]	500 $/kW$_{AC}$
Water electrolyzer Fixed operation and maintenance (FOM)[41]	25 $/kW-yr
Electrolyzer energy consumption[42]	47.6 MWh/ton H_2
Reactor cost[SI]	4750 $/m^2
Air separation unit (ASU) cost	150000 $/(ton N_2/hr)
ASU energy consumption[43]	0.29 MWh/ton N_2
Photovoltaic (PV) capital cost[44]	500 $/kW$_{AC}$
PV FOM[44]	5 $/kW-yr
Wind capital cost[44]	1200 $/kW$_{AC}$
Wind FOM[44]	24 $/kW-yr
Flash tank capital cost[SI]	1130 $/kW$_{th}$
Discount factor	8%
Contingency factor	21%
Plant lifetime	20 yrs
Target NH_3 discharge rate	250 ton NH_3/day (612 kmol/hr)
Battery storage capital cost[44]	116000 $/MWh
Battery power capital cost[44]	101000 $/MW
H_2 storage capital cost[45]	500000 $/(ton H_2)
H_2 power capital cost[45]	1200000 $/(ton H_2/hr)
N_2 storage capital cost[46]	1900 $/(ton H_2)
N_2 power capital cost[46]	476000 $/(ton H_2/hr)
NH_3 storage capital cost[47]	900 $/(ton NH_3)
NH_3 power capital cost[47]	120 $/(ton NH_3/hr)

Computational details

The power consumption of the reactor is a non-linear function of reactor size (specified by Ω^R) and production rate of ammonia at 100% Faradaic efficiency (x_t^{conv}), which can be related to the current density, $j_t = x_t^{conv}/\Omega^R$ (see model description below). As our approach involves formulating the design optimization problem as a MILP model, the power consumption must be linearized in two variables: reactor size and production rate at every time step. Several implementations for linearizing multivariate functions for use in MILP models have been proposed.[48] In this work, we implemented a simplex-based linearization, which allowed us to utilize a small number of binary variables to model a non-rectangular function domain for a function of two variables (see Fig. S4, SI for details).

The piece-wise linearization of the reactor power consumption function to production rate at each time step and reactor size introduces a large number of binary variables in the model: as described in SI, every time point introduces a set of approximately 15 binary variables for segment selection. It is desirable for the model to be able to utilize an entire year's worth of hourly power availability data to capture variability in power supply across multiple-time-scales. However, this corresponds to over 8000 individual time points; if every time point were to introduce 15 binary variables, then each model would contain over 100,000 binary variables, which would be prohibitively time-consuming to solve for each scenario and the limit the utility of the model for evaluating outcomes across a range of reactor parameter values.

In order to reduce the computational complexity of the design optimization model while not sacrificing accuracy of the reactor model, we only model plant operations over representative weeks that are identified from the original hourly power availability data for a year by applying k-means clustering.[49] The week used to represent each cluster of weeks in the design optimization model is chosen to be the week closest to the centroid of the cluster (Fig. S3). The quality of the temporal data reduction was assessed by simulating plant operations throughout the year to assess whether or not the optimized design can meet the specified ammonia demand across each hour. Not surprisingly, the amount of unmet or "slack" ammonia demand decreased when more representative weeks were used in the design optimization model, while the average computational time necessary to obtain an optimal model solution increased (Fig. S5). A balance of model accuracy and solution time was obtained when using 6 representative weeks (1008 hours), which corresponds to ~12% of the original data set of 52 weeks. All model runs were solved using Gurobi[50] on Xeon-g6 processor with 4 GB RAM per core on the MIT SuperCloud computing facility.[51] Solutions were obtained with a mixed integer program (MIP) optimality gap of 3%.

The overpotential of the electrochemical reactor was defined to be the difference between the total applied voltage and the sum of the thermodynamic potential and resistance losses at a total current density of 10 mA cm^{-2}, which is equivalent to the kinetic potential loss often used in the water splitting literature:[52]

$$\eta_R = \eta(j = 10\ mA\ cm^{-2}) = V - U_0 - R_{res} \cdot (10\ mA\ cm^{-2})$$

Mixed-integer linear programming model implementation

The sections below describe the equations used to implement of the MILP model. Tables S3-S5 define indexes, variables, and parameters used in the model. Parameters are fixed during a single model solution, but may change between different solution (e.g. the FE is a parameter that

is varied). Several mapping functions are used for implementing representative periods and electrochemical reactor power estimation – they are defined in the text when they are used.

Table S3 Definitions of indexes used throughout the MILP model.

Index set	Description
$t \in \mathcal{T}$	Index for modeled hours in the data series
$w \in \mathcal{W}$	Index for the representative periods in the model
$i \in \mathcal{I}$	Index for chemical species N_2, H_2, NH_3
$k \in \mathcal{K}$	Index for electrodes - a =anode, c = cathode
$r1, r2$	Reaction index, corresponding to NH_3 synthesis and H_2 recombination
$v \in \mathcal{V}$	Index for vertices used in function value estimation
$c \in \mathcal{C}$	Index for simplexes used in function value estimation
$s \in \mathcal{S}$	Type of storage technology
$s \in \mathcal{S}^B$	Electricity (battery) storage
$g \in \mathcal{G}$	Set of variable renewable generation technologies

Table S4. Definitions and units of parameters used throughout the MILP model.

Variable	Units	Description
$\rho_{g,t}^{CF}$	fraction	Capacity factor of electricity supply from resource $g \in \mathcal{G}$ at time index $t \in \mathcal{T}$
$\gamma^{k,r}$	fraction	Fraction of recycle stream to electrode k that is purged
γ^{FE}	fraction	Faradaic efficiency representing the share of electrons consumed by the NH_3 synthesis reaction
$\gamma^{P,LB}$	fraction	Lower bound for total plant ammonia output rate as a fraction of design flow rate (≤1; equal to 0.95 in our model)
$\gamma^{P,UB}$	fraction	Upper bound for total plant ammonia output rate as a fraction of design flow rate (≤1; equal to 1 in our model)
$\gamma^{P,AV}$	fraction	Minimum annual production commitment
DF	kmol/hr	Target NH_3 discharge rate
$\nu_i^{c,r1}$	-	Stoichiometric coefficients for the primary reaction on the cathode side, NH_3 synthesis (r1). H_2 = 0, N_2 = -1/2, NH_3 = 1
$\nu_i^{a,r1}$	-	Stoichiometric coefficients for the primary reaction on the anode, NH_3 synthesis (r1). H_2 = -3/2, N_2 = 0, NH_3 = 0
$\nu_i^{c,r2}$	-	Stoichiometric coefficients for secondary reaction at cathode, H_2 recombination (r2). H_2 = 3/2, N_2 = 0, NH_3 = 0

$\nu_i^{a,r2}$	-	Stoichiometric coefficients for secondary reaction at anode, H_2 recombination (r2). H_2 = -3/2, N_2 = 0, NH_3 = 0
η_s^C	fraction	Charging efficiency of storage type $s \in \mathcal{S}$
η_s^D		Discharging efficiency of storage type $s \in \mathcal{S}$
DF	ton/hr	Design ammonia flow rate from the facility
$p_g^{A,G}$	$/MW/yr	Annualized capital cost power generation for technology $g \in \mathcal{G}$
$p_s^{A,S,E}$	varied	Annualized capital cost per unit energy capacity for storage technology $s \in \mathcal{S}$. Units of $/MWh/yr for battery (electricity storage) or $/ton/yr for N_2, H_2, NH_3 storage.
$p_s^{A,S,P}$	varied	Annualized capital cost per unit power capacity for storage technology $s \in \mathcal{S}$. Units of $/MW/yr for battery (electricity storage) or $/(ton/hr)/yr for N_2, H_2, NH_3 storage.
$p^{A,WS}$	$/MW/yr	Annualized capital cost of PEM water splitting electrolyzer
$p^{A,ASU}$	$/(ton/hr)/yr	Annualized capital cost of PSA air separation units
$p^{A,LIQ,P}$	$/$MW_{th}$/yr	Annualized capital cost of NH_3 liquefaction loop refrigeration unit
$p^{A,LIQ,C}$	$/(kmol/hr)/yr	Annualized capital cost of NH_3 liquefaction loop mass capacity
$p^{A,R}$	$/$m^2$/yr	Annualized capital cost of electrochemical NH_3 synthesis reactor stacks
$p^{A,R,P}$	$/MW/yr	Annualized capital cost of electrochemical NH_3 synthesis reactor power supplies
$p^{A,R,G}$	$/(kmol/hr)/yr	Annualized capital cost of electrochemical NH_3 synthesis reactor gas distribution system
$p^{A,R,C}$	$/$MW_{th}$/yr	Annualized capital cost of electrochemical NH_3 synthesis reactor cooling heat exchangers
$p^{A,PRES,L}$	$/MW/yr	Annualized capital cost of liquid N_2 pump units
$p^{A,PRES,G}$	$/MW/yr	Annualized capital cost of gaseous N_2 compressor units
$p_g^{F,G}$	$/MW/yr	Fixed operation and maintenance (FOM) operating cost for power generation technology $g \in \mathcal{G}$
$p_s^{F,S,E}$	varied	FOM operating cost per unit energy capacity for storage technology $s \in \mathcal{S}$. Units of $/MWh/yr for battery (electricity storage) or $/ton/yr for N_2, H_2, NH_3 storage
$p_s^{F,S,P}$	varied	FOM operating cost per unit power for storage technology $s \in \mathcal{S}$. Units of $/MW/yr for battery (electricity storage) or $/(ton/hr)/yr for N_2, H_2, NH_3 storage
$p^{F,WS}$	$/MW/yr	FOM operating cost for PEM water splitting electrolyzer
$p^{F,ASU}$	$/(ton/hr)/yr	FOM operating cost for PSA air separation units
$p^{F,R}$	$/$m^2$/yr	FOM operating cost for electrochemical NH_3 synthesis reactor
$p_g^{V,G}$	$/MWh	Variable operating cost of generating power by resource $g \in \mathcal{G}$
$p_s^{V,S,c}$	varied	Variable operating cost for charging storage technology $s \in \mathcal{S}$. Units of $/MWh for battery (electricity) charge, $/ton for H_2, N_2, NH_3 charge

$p_s^{V,S,d}$	varied	Variable operating cost for discharging storage technology $s \in \mathcal{S}$. Units of \$/MWh for battery (electricity) discharge, \$/ton for H_2, N_2, NH_3 discharge
$p^{V,WS}$	\$/MWh	Variable operating cost for operating the PEM water electrolysis units, including feed water and cooling duty; values are effectively scaled to result in energy units
$p^{V,R}$	\$/MWh_{th}	Variable operating cost for operating the electrochemical NH_3 synthesis reactor, which mostly includes cooling duty
β_g^C	MWh/ton	Electricity consumption associated with charging N_2, H_2, NH_3 storage ($g \in \mathcal{S} \backslash \mathcal{S}^B$)
β_g^D	MWh/ton	Electricity consumption associated with discharging N_2, H_2, NH_3 storage ($g \in \mathcal{S} \backslash \mathcal{S}^B$). It is assumed to be non-zero only for N_2 discharge.
β^{ASU}	MWh/ton	Electricity consumption associated with producing N_2 using the PSA
β^{WS}	MWh/ton	Electricity consumption associated with producing H_2 using the water splitting PEM electrolyzer
$\beta_{N_2}^{PRES,G}$	MWh/ton	Electricity consumption associated with pressurizing N_2 from the ASU to reactor operating pressure
$\beta_{N_2}^{PRES,L}$	MWh/ton	Electricity consumption associated with pressurizing N_2 from storage to reactor operating pressure
$\beta_i^{HEAT,j}$	MWh/kmol	Electricity consumption for heating of species $i \in \mathcal{I}$ leaving unit j – one of N_2 storage, ASU, H_2 storage, WS. The values are computed outside of the model and account for the temperature change necessary. Computed in molar units as heat capacities of gases are more consistent between compounds than in mass units.
β_i^r	MWh_{th}/kmol	Sensible heat required to heat recycled species $i \in \mathcal{I}$ from liquefication unit to reactor temperature
H^{sep}	MWh/kmol	Energy consumption for NH_3 separation per mole of liquefied NH_3
H_{rxn}	MWh_{th}/kmol	Enthalpy of ammonia generation reaction under operating conditions – is typically negative, so heat is generated
$\chi_{sat}(T,P)$	fraction	Mole fraction of ammonia in the gas phase as a function of temperature and pressure
μ_i	ton/kmol	Molecular weight of species $i \in \mathcal{I}$
w_t	hr/yr	Weighting of time index $t \in \mathcal{T}$ from representative week selection. This is unique for any set of VRE availability data.
f_k	-	Fraction of material purged from electrode k of the electrochemical reactor. Assumed to be 0.01 for the cathode, 0 for the anode.
p_{bat}^{dur}	h	Upper bound for battery storage duration
p^{cool}	MW/MW_{th}	Electricity requirement per MW_{th} necessary to be removed in liquefication unit (refrigeration cycle efficiency)
P_v^{val}	MW	Power consumption of the electrochemical reactor at vertex v
A_v^{val}	m^2	Total reactor area of the electrochemical reactor at vertex v
χ_v^{val}	kmol/hr	Production rate of the electrochemical reactor at vertex v

p_{maxj}	A/m^2	Maximum allowable current density in reactor
p^{slack}	$/ton	Cost of imaginary, slack ammonia used in plant simulation. The cost is a fixed high value (e.g. 1000x a typical ammonia cost)
n_h	-	Number of hours per representative period
n_w	-	Number of representative periods
n_D	hr	Minimum duration of downtime period in hours

Table S3. Definitions and units of variables used throughout the MILP model.

Variable	Units	Description
$\Omega_g^G \in \mathbb{R}_+$	MW	Installed generation capacity of technology $g \in \mathcal{G}$
$\Omega_s^{S,E} \in \mathbb{R}_+$	varied	Installed energy storage capacity of technology $s \in S$. Units of MWh for battery (electricity storage) or ton for N_2, H_2, NH_3 storage.
$\Omega_s^{S,P} \in \mathbb{R}_+$	varied	Installed power capacity of technology $s \in S$. Units of MW for battery (electricity storage) or ton/hr for N_2, H_2, NH_3 storage
$\Omega^{WS} \in \mathbb{R}_+$	MW	Installed PEM water splitting electrolyzer capacity
$\Omega^{ASU} \in \mathbb{R}_+$	ton/hr	Installed PSA air separation capacity
$\Omega^{R} \in \mathbb{R}_+$	m^2	Installed electrochemical NH_3 synthesis reactor size – total stack area
$\Omega^{R,P} \in \mathbb{R}_+$	MW	Maximum power consumption of electrochemical NH_3 synthesis reactor
$\Omega^{R,G} \in \mathbb{R}_+$	kmol/hr	Maximum gas flowrate through electrochemical NH_3 synthesis reactor
$\Omega^{R,C} \in \mathbb{R}_+$	MW_{th}	Maximum cooling duty consumption of electrochemical NH_3 synthesis reactor
$\Omega^{LIQ,C} \in \mathbb{R}_+$	kmol/hr	Installed NH_3 liquefication unit mass capacity
$\Omega^{LIQ,P} \in \mathbb{R}_+$	MW_{th}	Maximum thermal load of NH_3 liquefication unit
$\Omega^{PRES,L} \in \mathbb{R}_+$	MW	Installed liquid N_2 pressurization (pump) capacity
$\Omega^{PRES,G} \in \mathbb{R}_+$	MW	Installed gaseous N_2 pressurization (compressor) capacity
$\Theta_{g,t}^G \in \mathbb{R}_+$	MW	Power supplied by technology $g \in \mathcal{G}$ at time index $t \in \mathcal{T}$
$\Theta_{s,t}^D \in \mathbb{R}_+$	varied	Rate of energy discharge for storage technology $s \in \mathcal{S}$ at time index $t \in \mathcal{T}$. Units of MW for battery (electricity) charging, ton/hr for H_2, N_2, NH_3 discharging
$\Pi_{s,t}^C \in \mathbb{R}_+$	varied	Rate of energy charge (energy consumption) for storage technology $s \in \mathcal{S}$ at time index $t \in \mathcal{T}$. Units of MW for battery (electricity) charging, ton/hr for H_2, N_2, NH_3 charging
$\Pi_t^{WS} \in \mathbb{R}_+$	MW	Power consumption of the PEM water splitting electrolyzer at time index $t \in \mathcal{T}$
$\Pi_t^{R} \in \mathbb{R}_+$	MW	Power consumption of the electrochemical NH_3 synthesis reactor at time index $t \in \mathcal{T}$
$\Pi_t^{R,C} \in \mathbb{R}_+$	MW_{th}	Cooling duty requirement (i.e. cooling water) of the electrochemical NH_3 synthesis reactor at time index $t \in \mathcal{T}$
$\Pi_t^{LIQ} \in \mathbb{R}_+$	MW	Power consumption of the NH_3 liquefication unit at time index $t \in \mathcal{T}$
$\Pi_t^{PRES} \in \mathbb{R}_+$	MW	Power consumption of the pressurization units at time index $t \in \mathcal{T}$
$\Pi_t^{HEAT} \in \mathbb{R}_+$	MW	Power consumption of the gas preheater units at time index $t \in \mathcal{T}$

$F_{i,t}^{k,p} \in \mathbb{R}_+$	kmol/hr	Flow rate of species i from production unit $p \in \{WS, ASU\}$ to electrode k at time index $t \in \mathcal{T}$
$F_{i,t}^{k,s} \in \mathbb{R}_+$	kmol/hr	Flow rate of species i from storage unit s to electrode k at time index $t \in \mathcal{T}$
$F_{i,t}^{k,r} \in \mathbb{R}_+$	kmol/hr	Recycle flow rate of species i to electrode k at time index $t \in \mathcal{T}$
$F_{i,t}^{k,f} \in \mathbb{R}_+$	kmol/hr	Feed flow rate of species i to electrode k at time index $t \in \mathcal{T}$
$F_{i,t}^{k,o} \in \mathbb{R}_+$	kmol/hr	Outlet flow rate of species i from electrode k at time index $t \in \mathcal{T}$
$F_{i,t}^{sep,p} \in \mathbb{R}_+$	kmol/hr	Liquid product flow rate of species i from the separator as the product at time index $t \in \mathcal{T}$
$F_t^{slack} \in \mathbb{R}_+$	kmol/hr	Unmet ammonia flowrate used to close mass balances during full-year simulations of the production plant
$S_{s,t}^{soc} \in \mathbb{R}_+$	varied	State of charge of storage $s \in \mathcal{S}$ at time index $t \in \mathcal{T}$. Units of MWh for battery storage, ton for H_2, N_2, and NH_3 storage.
$S_{s,\mathrm{w}}^{soc,init} \in \mathbb{R}_+$	varied	State of charge of storage $s \in \mathcal{S}$ at the beginning of the representative period $w \in \mathcal{W}$. Units of MWh for battery storage, ton for H_2, N_2, and NH_3 storage.
$S_{s,w}^{BU} \in \mathbb{R}$	varied	Build-up of state of charge of storage $s \in \mathcal{S}$ for representative period $w \in \mathcal{W}$. Units of MWh for battery storage, ton for H_2, N_2, and NH_3 storage.
$x_t^{conv} \in \mathbb{R}_+$	kmol/hr	Production rate of ammonia at 100% Faradaic efficiency at time period t
T_t	ton/hr	Total ammonia output from plant at time index $t \in \mathcal{T}$
$\alpha_{v,t} \in \mathbb{R}_+$	-	Fraction of vertex v used to estimate reactor power consumption in period t
$h_{c,t} \in \{0,1\}$	-	Binary variable representing whether a given simplex c is active for reactor power estimation at time index $t \in \mathcal{T}$
$\Lambda_t \in \{0,1\}$	-	Binary variable representing whether the electrochemical NH_3 synthesis reactor is on (active) at time index $t \in \mathcal{T}$
$\xi_t \in \{0,1\}$	-	Binary variable representing whether the entire plant is active (outputting NH_3) at time index $t \in \mathcal{T}$
$\xi_t^D \in \mathbb{R}_+$	-	Binary variable (though need not be represented as one) representing whether the entire plant is shutting down at time index $t \in \mathcal{T}$
$\xi_t^U \in \{0,1\}$	-	Binary variable (though need not be represented as one) representing whether the entire plant is starting up at time index $t \in \mathcal{T}$
$A_t' \in \mathbb{R}_+$	m^2	A helper variable representing the product of the continuous variable Ω^R and binary variable Λ_t

Representative weeks for reducing problem size

The number of variables in the MILP model scale directly with the number of hours of plant operation considered as well as with the problem complexity. In particular, the use of binary

variables to model time-dependent operation of the electrochemical reactor (see below) significantly increases the time necessary to solve the model, making it impractical to model a full year of plant operation at an hourly resolution. This also makes it difficult to use the model for carrying out a full factorial analysis to understand the impact of various reactor parameters on the levelized cost of ammonia.

To reduce the model complexity, we reduced the number of time points used when sizing the plant using a representative time period approach.[53] In this approach, the dataset of interest, which, in this case, is the variation in renewable power availability, is reduced to a few weighted representative time periods that can fairly accurately model the rest of the dataset. In our model, we chose to select some weeks of the year that can accurately represent all 52 weeks when appropriately weighted (Fig. S3). This was done by using K-means clustering, from which several most representative weeks were obtained. For example, if we use photovoltaic energy availability data from New York and attempt to reduce the data to two representative weeks, we obtain an "average" winter week, as well as an "average" summer week, with 28 to 24 weighting (Fig. S3). In practice, more than two representative weeks are used in more accurate models.

During the process of selecting representative weeks to reduce the resolution of the data, some information is inevitably lost. Looking back at the two-week representation of the New York solar availability data (Fig. S3), we can anticipate that the power availability data for the spring and fall seasons are not captured, as well as the random variation in cloudy days that may occur during any season. One solution to this is to increase the number of representative weeks used. This improves the data representation quality, and thus increases model accuracy. However, the complexity of the model is also increased, which leads to increased solve times. To assess whether the results obtained using the representative week solution are valid, we fixed the size of the plant at the optimized values and performed a simulation over the entire year. These simulations are much faster than plant sizing as the number of independent variables is significantly reduced. To allow for erroneously sized plants to lead to feasible solutions, we relax the constraint necessitating a constant output rate of ammonia (Eq. 6 and Eq. 7 below). Instead, we allow some slack in the ammonia output which is heavily penalized. The cost of underproduction of ammonia is typically 1000 times higher (~1000 $/kg) than the final cost of producing ammonia.

We varied the number of representative weeks used to size the plant and ran simulations over the entire data set (Fig. S5). We found that increasing the number of representative weeks increased the maximum optimization time significantly (though some simulations still converged rapidly), while the fraction of ammonia that had to be accounted for via the slack variable decreased. The lower the amount of ammonia that must be obtained via slack, the more appropriate the plant sizing is for the renewable energy availability at hand. Low slack values mean that the representative weeks chosen are accurate representations of the entire yearly energy availability. When using 6 representative weeks (11.5% of the total renewable availability data), very little ammonia had to be derived from the slack, while simulation times were quite low, which suggests that using 6 representative weeks for sizing the plant strikes a balance between problem complexity and result accuracy. The optimum number of representative weeks changed with location and power source, typically being higher for wind, due to its more random power production. However, 6 weeks were used in the vast majority of simulations in this work.

In the model, the representative periods all have the same number of hours (though might have different weights), are indexed starting at 1. For example, if representative periods are 24 hours long, then time index 77 is hour 5 in representative period 3.

Objective function

The objective function minimizes the sum of all capital and operating costs for all units. When computing operating costs, time intervals are weighted by the occurrence of representative weeks (w_t) that was obtained in the data simplification process.

$$\begin{aligned} f = & \sum_{g \in \mathcal{G}} \left(\left(p_g^{A,G} + p_g^{F,G} \right) \cdot \Omega_g^G \right) \\ & + \sum_{s \in \mathcal{S}} \left(\left(p_s^{A,S,E} + p_s^{F,S,E} \right) \cdot \Omega_s^{S,E} + \left(p_s^{A,S,P} + p_s^{F,S,P} \right) \cdot \Omega_s^{S,P} \right) \\ & + \left(p^{A,WS} + p^{F,WS} \right) \cdot \Omega^{WS} + \left(p^{A,ASU} + p^{F,ASU} \right) \cdot \Omega^{ASU} \\ & + \left(p^{A,LIQ,P} \cdot \Omega^{LIQ,P} + p^{A,LIQ,C} \cdot \Omega^{LIQ,C} \right) \\ & + \left(p^{A,PRES,G} \cdot \Omega^{PRES,G} + p^{A,PRES,L} \cdot \Omega^{PRES,L} \right) + C^R + C^{VOM} \end{aligned} \quad \text{Eq. 1}$$

The variable operation and maintenance (VOM) costs come from operating the various unit operations in the plant:

$$\begin{aligned} C^{VOM} = & \sum_{g \in \mathcal{G}} \sum_{t \in \mathcal{T}} \left(p_g^{V,G} \cdot \Theta_{g,t}^G \cdot w_t \right) + \sum_{s \in \mathcal{S}} \sum_{t \in \mathcal{T}} \left(p_s^{V,S,c} \cdot \Pi_{s,t}^C \cdot w_t + p_s^{V,S,d} \cdot \Theta_{s,t}^D \cdot w_t \right) \\ & + \sum_{t \in \mathcal{T}} \left(p^{V,WS} \cdot \Pi_t^{WS} \cdot w_t \right) + \sum_{t \in \mathcal{T}} \left(p^{V,R} \cdot \Pi_t^{R,C} \cdot w_t \right) \end{aligned} \quad \text{Eq. 2}$$

The reactor cost breakdown is discussed in the section devoted to reactor modeling.

The objective function of the MILP model is the annualized cost of the facility shown in Figure 1, which is minimized. The total cost is composed of several capital cost terms, which account for all fixed part of the process, including variable renewable energy (VRE) sources, reactors, and separators, and a variable operating cost term, which accounts for continuous resource use, such as cooling water and grid electricity. The lifetime of most fixed parts of the process is assumed to be 20 years when calculating annualized costs. The plant is designed to output 250 ton day^{-1} of ammonia continuously independent of renewable energy availability, which it can do by producing NH_3 in an electrochemical reactor or discharging stored ammonia which was synthesized at an earlier time.

When simulating reactor operation for an entire year with fixed sizing (as opposed to sizing the plant based on limited representative weeks), the objective function has an additional slack parameter (Eq. 3), the value of which is computed from system-level constraints:

$$f_{slack} = f + C_{slack} \quad \text{Eq. 3}$$

System-level constraints

Eq. 4 represents the power balance constraint, which ensures that electricity generation and consumption are balanced at each time step:

$$\sum_{g\in\mathcal{G}} \Theta_{g,t}^{G} + \sum_{s\in\mathcal{S}^B} \left(\Theta_{s,t}^{D} - \Pi_{s,t}^{C}\right) = \Pi_t^{WS} + \Pi_t^{ASU} + \Pi_t^{R} + \Pi_t^{PRES} + \Pi_t^{HEAT} + \Pi_t^{LIQ} + \sum_{s\in\mathcal{S}\setminus\mathcal{S}^B} \left(\beta_g^{D}\cdot\Theta_{s,t}^{D} + \beta_g^{C}\cdot\Pi_{s,t}^{C}\right) \quad \text{Eq. 4}$$

Eq. 5 defines the production rate of ammonia over the entire plant.

$$\mu_{NH_3}\cdot F_{NH3,t}^{sep,p} + \Theta_{NH3,t}^{D} = T_t \;\; \forall t\in\mathcal{T} \quad \text{Eq. 5}$$

In the case of whole-year simulations of the plant, the production rate of ammonia is defined by Eq. 6, while the cost of the slack ammonia is computed via Eq. 7.

$$\mu_{NH_3}\cdot F_{NH3,t}^{sep,p} + \Theta_{NH3,t}^{D} + \mu_{NH_3}\cdot F_t^{slack} = T_t \;\; \forall t\in\mathcal{T} \quad \text{Eq. 6}$$

$$C_{slack} = \sum_{t\in\mathcal{T}} p^{slack}\cdot\mu_{NH_3}\cdot F_t^{slack} \;\; \forall t\in\mathcal{T} \quad \text{Eq. 7}$$

Eq. 8, Eq. 9, Eq. 10 represent the required minimum and maximum plant ammonia production rates when the plant is active, as well as the necessary total yearly ammonia production.

$$T_t \geq DF\cdot\gamma^{P,LB}\cdot\xi_t \;\; \forall t\in\mathcal{T} \quad \text{Eq. 8}$$

$$T_t \leq DF\cdot\gamma^{P,UB}\cdot\xi_t \;\; \forall t\in\mathcal{T} \quad \text{Eq. 9}$$

$$\sum_{t\in\mathcal{T}} T_t\cdot w_t \geq \sum_{t\in\mathcal{T}} DF\cdot\gamma^{P,UB}\cdot w_t \quad \text{Eq. 10}$$

Eq. 11 and Eq. 12 define variables for accounting for plant startup and shutdown.

$$\xi_t - \xi_{(n_h+1)\cdot(f_p(t)-1)} = \xi_t^U - \xi_t^D \quad \forall t\in\mathcal{T}: f_h(t) = 1 \quad \text{Eq. 11}$$

$$\xi_t - \xi_{t-1} = \xi_t^U - \xi_t^D \quad \forall t\in\mathcal{T}: f_h(t) \neq 1 \quad \text{Eq. 12}$$

Here $f_p(t)$ maps time index t to its representative period, while $f_h(t)$ maps time index t to the hour it represents in its representative period. Eq. 11 applies in the case where the time index of interest is at the beginning of its representative period. In this case, we must compare the plant commitment at the first ($t: f_h(t) = 1$) and last ($t = (n_h + 1)\cdot\left(f_p(t) - 1\right)$) time indexes of the representative period.

Equations Eq. 13 and Eq. 14 necessitate that if the plant is shut down, it must be down for at least a finite amount of time defined by n_D. The two equations account for required differences in time index numeration for various parts of a representative period.

$$1 - \xi_t \geq \sum_{i=t-f_h(t)+1}^{t} \xi_i^D + \sum_{i=n_h-n_D+f_h(t)}^{n_h} \xi_i^D \quad \forall t\in\mathcal{T}: f_h(t) \leq n_D \quad \text{Eq. 13}$$

$$1 - \xi_t \geq \sum_{i=t-n_D}^{t} \xi_i^D \quad \forall t \in \mathcal{T}: f_h(t) > n_D \qquad \text{Eq. 14}$$

Power supply and storage constraints

The amount of power that can be produced by any given power sources is given by Eq. 15. Note that this implementation allows for curtailment of installed capacity.

$$\Theta_{g,t}^G \leq \rho_{g,t}^{CF} \cdot \Omega_g^G \ \ \forall g \in \mathcal{G}, \forall t \in \mathcal{T} \qquad \text{Eq. 15}$$

The change state of charge in time of various kinds of storage is accounted for in Eq. 16 and Eq. 17. Material storage is modeled for each time step. For every hour, the material (H_2, N_2, NH_3) can enter or leave the storage at any rate chosen by the model. Eq. 17 loops the storage capacity for each representative period if the time index is at the beginning of the representative period. These equations implicitly assume a 1 hr time for charging and discharging (for unit consistency).

Material storage is modeled for each time step. For every hour, the material (H_2, N_2, NH_3) can enter or leave the storage at any rate chosen by the model. The capital cost of storage is defined by a sum of maximum capacity necessary (e.g. tank size) and the maximum rate of change necessary (e.g. pump size). Similar modeling is done for the electrical storage in batteries.

$$S_{s,t}^{soc} = S_{s,t-1}^{soc} + \eta_s^C \cdot \Pi_{s,t}^C - \eta_s^D \cdot \Theta_{s,t}^D \ \ \forall t \in \mathcal{T}: f_h(t) \neq 1, s \in \mathcal{S} \qquad \text{Eq. 16}$$

$$S_{s,t}^{soc} = S_{s,n_h \cdot f_p(t)}^{soc} - S_{s,f_p(t)}^{soc,BU} + \eta_s^C \cdot \Pi_{s,t}^C - \eta_s^D \cdot \Theta_{s,t}^D \quad \forall t \in \mathcal{T}: f_h(t) = 1, s \in \mathcal{S} \qquad \text{Eq. 17}$$

Eq. 18, Eq. 19, Eq. 20, Eq. 21 define the sizing of storage and power capacity for the forms of energy storage. Note that battery storage has symmetric charging and discharging, and has a linear relationship between storage capacity and power. Physical storage does not have these limitations.

$$\Pi_{s,t}^C \leq \Omega_s^{S,P} \ \ \forall s \in \mathcal{S}, \forall t \in \mathcal{T} \qquad \text{Eq. 18}$$

$$\Theta_{s,t}^D \leq \Omega_s^{S,P} \ \ \forall s \in \mathcal{S}^B, \forall t \in \mathcal{T} \qquad \text{Eq. 19}$$

$$S_{s,t}^{soc} \leq \Omega_s^{S,E} \ \ \forall s \in \mathcal{S}, \forall t \in \mathcal{T} \qquad \text{Eq. 20}$$

$$\Omega_s^{S,E} \leq p_{bat}^{dur} \cdot \Omega_s^{S,P} \ \ \forall s \in \mathcal{S}^B, \forall t \in \mathcal{T} \qquad \text{Eq. 21}$$

Eq. 22 defines that the initial storage level for all forms of storage at the beginning of a representative period must be consistent with the change in level of storage over the period. The $w + 1 \bmod n_w$ notation loops the representative period, with the initial storage level of the first representative period being dependent on the last's one. Eq. 23 computes the storage level build-

ups over the representative period using index indexes. Eq. 24 maintains that the initial state of charge in each representative period does not exceed installed storage capacity.

$$S^{soc,init}_{s,(w+1 \bmod n_w)} = S^{soc,init}_{s,w} + S^{BU}_{g,w} \;\; \forall s \in \mathcal{S}, \forall w \in \mathcal{W} \quad \text{Eq. 22}$$

$$S^{soc,init}_{s,w} = S^{soc}_{s,n_h \cdot w} - S^{BU}_{s,w} \;\; \forall s \in \mathcal{S}, \forall w \in \mathcal{W} \quad \text{Eq. 23}$$

$$S^{soc,init}_{s,w} \leq \Omega^{S,E}_{s} \;\; \forall s \in S, \forall w \in \mathcal{W} \quad \text{Eq. 24}$$

Water electrolyzer and air separation units

PEM water splitting electrolysis and PSA air separation are used to produce H_2 and N_2 respectively. Since the focus of the study on the electrochemical reactor modeling, we use simplified models for water spitting and air separation units, wherein their specific energy consumption (MWh/ton of product produced) is assumed to not vary with extent of utilization of the unit. The produced gases can either be sent to storage or to the electrochemical reactor. The N_2 is sent to the cathode compartment of the electrochemical reactor, while H_2 is sent to the anode compartment. Both units are sized according to the maximum production rate necessary.

$$\Pi^{WS}_{t} = \beta^{WS} \cdot \left(F^{c,WS}_{H_2,t} \cdot \mu_{H_2} + \Pi^{C}_{s,t}\right) \;\; \forall t \in \mathcal{T}, s \in \mathcal{S}^{H_2} \quad \text{Eq. 25}$$

$$\Pi^{WS}_{t} \leq \Omega^{WS} \;\; \forall t \in \mathcal{T} \quad \text{Eq. 26}$$

$$\Pi^{ASU}_{t} = \beta^{ASU} \cdot \left(F^{c,ASU}_{N_2,t} \cdot \mu_{N_2} + \Pi^{C}_{s,t}\right) \;\; \forall t \in \mathcal{T}, s \in \mathcal{S}^{N_2} \quad \text{Eq. 27}$$

$$\Pi^{ASU}_{t} \leq \Omega^{ASU} \;\; \forall t \in \mathcal{T} \quad \text{Eq. 28}$$

Gas pressurization and preheating

The gas entering the electrochemical reactor is pressurized and heated to the reactor conditions, which requires electrical energy and additional equipment.

Eq. 29 shows the power consumption for pressurizing gaseous nitrogen leaving the ASU and liquid nitrogen leaving storage to the operating pressure. Note that because hydrogen is assumed to be stored at pressure, hydrogen pressurization is accounted for when computing storage power requirements, and is not explicitly accounted for.

$$\Pi^{PRES}_{t} = F^{c,ASU}_{N_2,t} \cdot \mu_{N_2} \cdot \beta^{PRES,G}_{N_2} + \Theta^{D}_{s,t} \cdot \beta^{PRES,L}_{N_2} \;\; \forall t \in \mathcal{T}, s \in \mathcal{S}^{N_2} \quad \text{Eq. 29}$$

Eq. 30 and Eq. 31 are used to size the liquid nitrogen pump and gaseous nitrogen compressor, respectively.

$$\Theta^{D}_{s,t} \cdot \beta^{PRES,L}_{N_2} \leq \Omega^{PRES,L} \;\; \forall t \in \mathcal{T} \quad \text{Eq. 30}$$

$$F_{N_2,t}^{c,ASU} \cdot \mu_{N_2} \cdot \beta_{N_2}^{PRES,G} \leq \Omega^{PRES,G} \quad \forall t \in \mathcal{T} \qquad \text{Eq. 31}$$

Eq. 32 accounts for the power requirements for heating gases leaving storage or unit operations to reactor temperature:

$$\Pi_t^{HEAT} = \beta_{N_2}^{HEAT,ASU} \cdot F_{N_2,t}^{c,ASU} + \beta_{N_2}^{HEAT,N_2stor} \cdot \frac{\Theta_{N_2,t}^{D}}{\mu_{N_2}} + \beta_{H_2}^{HEAT,WS} \cdot F_{H_2,t}^{c,WS} + \beta_{H_2}^{HEAT,H_2stor} \cdot \frac{\Theta_{H_2,t}^{D}}{\mu_{H_2}} \cdot \quad \forall t \in \mathcal{T} \qquad \text{Eq. 32}$$

Modeling the separations system

The synthesis loop contains a unit operation to remove NH_3 from the product stream. We assumed that the ammonia is removed from the gas stream by liquefication at -30 °C in a flash drum. Liquefication at these temperatures can be done with fairly routine equipment (e.g. an ammonia-based cooling system). The separation of ammonia from the other gaseous species can be modeled by using assuming a vapor-liquid equilibrium in the unit. The amount of ammonia in the gas stream is a function of the temperature and pressure in the drum and of the flowrate of the non-ammonia gases entering the flash tank. If less ammonia than necessary for saturation enters the flash tank, then all the ammonia entering the flash tanks leaves the tank with the gas stream. Assuming that some ammonia is liquefied, the separation mass balance is defined in Eq. 33:

$$F_{NH_3,t}^{a,r} = \chi_{sat}(T,P) \cdot \sum_{i \in \mathcal{I}} F_{i,t}^{c,o} \quad \forall t \in \mathcal{T} \qquad \text{Eq. 33}$$

The amount of ammonia in the liquid stream from the separator can be found via Eq. 34, which is a mass balance over the separator:

$$F_{NH_3,t}^{a,r} + \frac{\Pi_{NH_3,t}^{C}}{\mu_{NH_3}} + F_{NH_3,t}^{sep,p} = F_{NH_3,t}^{c,o} \quad \forall t \in \mathcal{T} \qquad \text{Eq. 34}$$

Similarly, Eq. 35 is a mass balance over the nitrogen and hydrogen, assuming that negligible amounts of nitrogen or hydrogen dissolve in the ammonia:

$$F_{i,t}^{a,r} = F_{i,t}^{c,o} \quad \forall t \in \mathcal{T}, i \in \{H_2, N_2\} \qquad \text{Eq. 35}$$

The cooling duty for the flash unit can be computed by accounting for energy needed to cool incoming gases to the flash temperature (sensible heat) and the energy needed to liquefy the ammonia (latent heat). The gas-cooling coefficient, β_i^r, is a function of reactor and flash unit temperatures, while the latent heat of ammonia condensation, H^{sep}, is approximately constant with temperature. The cooling duty can be converted to the electricity consumption by including the refrigeration cycle efficiency, as seen in Eq. 36:

$$\Pi_t^{LIQ} \cdot \frac{1}{p^{cool}} = \sum_{i \in \mathcal{I}} \beta_i^r \cdot F_{i,t}^{c,o} + H^{sep}\left(\frac{\Pi_{NH_3,t}^{C}}{\mu_{NH_3}} + F_{NH_3,t}^{sep,p}\right) \quad \forall t \in \mathcal{T} \qquad \text{Eq. 36}$$

The saturation pressure of ammonia $\chi_{sat}(T,P)$, as well as the gas-cooling coefficients β_i^r and latent heat of ammonia condensation H^{sep} were estimated using Aspen Plus thermodynamic modeling.

The gases in the flash unit are cooled using a refrigerator the cost of which is proportional to the maximum cooling duty necessary. The maximum cooling duty is defined by Eq. 37:

$$\Pi_t^{LIQ} \leq \Omega^{LIQ,P} \quad \text{Eq. 37}$$

The liquefication unit must also have a physical capacity to allow for accumulation and cooling of ammonia. To cost the tank, the volume of the tank must be estimated. Typically, the volume of a flash tank is a function of the volume of liquid in the tank (i.e. liquid takes up ~30% of the volume).[54] The volume of liquid depends on the flow rate and residence time of the liquid. The residence time is assumed to be ~10 minutes. Knowing the flow rate of liquid into the tank, the liquid volume, a flash tank volume can be computed. The size of the tank is defined in Eq. 38:

$$\frac{\Pi_{NH_3,t}^{C}}{\mu_{NH_3}} + F_{NH_3,t}^{sep,p} \leq \Omega^{LIQ,C} \quad \text{Eq. 38}$$

Modeling the electrochemical reactor

The electrochemical ammonia synthesis reactor is the key part of the plant and needs to be modeled in greater detail. As it is not clear what chemistry would be ultimately used in an industrial setting for producing ammonia electrochemically, we modeled the reactor as a generic electrochemical system for which various parameters can be assumed. Several equations describing inflow and outflow to the reactor, as well as its power and cooling consumption are described below.

Eq. 39 represents the inlet mass balances for the anode compartment over hydrogen:

$$F_{H_2,t}^{a,WS} + \frac{\Theta_{H_2,t}^{D}}{\mu_{H_2}} + (1 - f_a) \cdot F_{H_2,t}^{a,r} = F_{H_2,t}^{a,f} \quad \forall t \in \mathcal{T} \quad \text{Eq. 39}$$

Eq. 40 represents the inlet mass balances for the anode compartment over nitrogen and ammonia:

$$(1 - f_a) \cdot F_{i,t}^{a,r} = F_{i,t}^{a,f} \quad \forall t \in \mathcal{T}, i \in \{N_2, NH_3\} \quad \text{Eq. 40}$$

Eq. 41 represents the inlet mass balance for the cathode compartment over nitrogen:

$$F_{N_2,t}^{c,ASU} + \frac{\Theta_{s,t}^{D}}{\mu_{N_2}} + (1 - f_c) \cdot F_{N_2,t}^{c,r} = F_{N_2,t}^{c,f} \quad \forall t \in \mathcal{T}, s \in \mathcal{S}^{N_2} \quad \text{Eq. 41}$$

Eq. 42 represents the inlet mass balances for the cathode compartment over hydrogen and ammonia:

$$(1 - f_c) \cdot F_{i,t}^{c,r} = F_{i,t}^{c,f} \quad \forall t \in \mathcal{T}, i \in \{H_2, NH_3\} \quad \text{Eq. 42}$$

Eq. 43 represents the mass balance at the cathode and anode side of the reactor accounting for conversion of reactants via primary (ammonia synthesis) and secondary reactions (hydrogen recombination). We define reaction conversion (x_t^{conv}) based on the ammonia production rate at 100% Faradaic efficiency, while the Faradaic efficiency is an independent parameter that is explicitly defined.

$$F_{i,t}^{k,o} = F_{i,t}^{k,f} + \gamma^{FE} \nu_i^{k,r1} x_t^{conv} + (1-\gamma^{FE}) \nu_i^{k,r2} x_t^{conv} \quad \forall t \in \mathcal{T}, i \in \mathcal{I}$$ Eq. 43

Eq. 44 enforces that the output flow rate from the anode is equal to the flow rate of the recycle stream to the cathode inlet, not accounting for the purge flow rate, which is accounted for in the feed to the cathode.

$$F_{i,t}^{a,o} = F_{i,t}^{c,r}$$ Eq. 44

Eq. 45 is used to find the maximum power consumption of the reactor, which is used to size power electronics.

$$\Pi_t^R \leq \Omega^{R,P} \quad \forall t \in \mathcal{T}$$ Eq. 45

Eq. 46 accounts for the amount cooling necessary to maintain the reactor at constant temperature. The reactor produces heat from electrical losses and from the enthalpy of ammonia formation, while heat is used to heat recycled gases back to reactor temperature.

$$\Pi_t^{R,C} = \Pi_t^R + (-H_{rxn}) \cdot x_t^{conv} \cdot \gamma^{FE} - \sum_{i \in \mathcal{I}} F_{i,t}^{a,R} \cdot \beta_i^r \quad \forall t \in \mathcal{T}$$ Eq. 46

Eq. 47 is used to find the maximum cooling duty necessary, which is used to size the reactor heat exchangers.

$$\Pi_t^{R,C} \leq \Omega^{R,C} \quad \forall t \in \mathcal{T}$$ Eq. 47

Eq. 48 is used to find the maximum gas flowrate through the reactor, which is used to size gas manifolds:

$$\sum_{k \in \{a,c\}} \sum_{i \in \mathcal{I}} F_{i,t}^{k,f} + F_{i,t}^{k,r} \leq \Omega^{R,G} \quad \forall t \in \mathcal{T}$$ Eq. 48

The reactor fixed cost is broken down into stack costs and balance of plant (BOP) costs (Eq. 49). BOP costs include power supplies (AC to DC), gas manifolds, and heat exchangers for reactor cooling:

$$C^R = p^{A,R} \cdot \Omega^R + p^{A,R,G} \cdot \Omega^{R,G} + p^{A,R,P} \cdot \Omega^{R,P} + p^{A,R,C} \cdot \Omega^{R,C}$$ Eq. 49

Eq. 50 is constraint that limits the overall current density over the plant; this implicitly assumes that the current density in all cells is identical. F_{far} is Faraday's constant in appropriate units. This constraint is typically redundant, as the domain of allowable total electrode areas and production rates is defined by the maximum allowable current density (see below).

$$x_t^{conv} \leq \frac{\Omega^R \cdot p_{maxj}}{3 \cdot F_{far}} \quad \forall t \in \mathcal{T}$$ Eq. 50

Linearization of power consumption

We would like to estimate the power consumption of the reactor as a function of reactor size (Ω^R) and ammonia production rate (x_t^{conv}). However, the power consumption is a non-linear

function of both variables, and thus cannot be used directly in the MILP model. Therefore, we must linearize the power consumption to use it in the model. To accurately capture some of the non-linear behavior of the power dependence on process parameters, a piecewise implementation must be used.

The function of interest effectively has two independent variables: the total electrode area and the production rate of ammonia. Several methods for piecewise linearization of functions of two variables have been reported, though some of them lead to non-continuous function values.[48] We used a generalizable approach in which the surface representing the function in area-rate-power space was represented by a set of connected triangles, or simplexes, similar to how 3-dimensional models are represented in computer graphics and computational fluid dynamics applications. In this implementation, the power consumption is computed at a number of production rate-area points called vertices. The formulas used to compute the power consumption are described in the following section. The vertices are grouped into groups of three points called simplexes (Fig. S4). Each simplex represents a triangle on the function surface; the power consumption can be estimated to be a linear interpolation of the three vertices if the independent variable values lie inside the triangle defined by the simplex. The vertex electrode areas, production rates, and power consumptions are fed as parameters to the MILP model ($A_v^{val}, \chi_v^{val}, P_v^{val}$), while the simplexes (grouping of vertices) are fed as a mapping function.

In the model implementation, every vertex has an associated variable which represents a weight (α_v), which can take a value between 0 and 1. Every simplex has an associated binary variable (h_s), which can take a non-zero value if the rate and area for which the power consumption needs to be computed lie inside the simplex. The values for the power consumption (Eq. 51), production rate (Eq. 52), and reactor area (Eq. 53) are found by computing the sum of every vertex's value of the respective variable, weighted by the vertex weight:

$$\Pi_t^R = \sum_{v \in \mathcal{V}} \alpha_{v,t} \cdot P_v^{val} \quad \forall t \in \mathcal{T} \qquad \text{Eq. 51}$$

$$x_t^{conv} = \sum_{v \in \mathcal{V}} \alpha_{v,t} \cdot \chi_v^{val} \quad \forall t \in \mathcal{T} \qquad \text{Eq. 52}$$

$$A_t' = \sum_{v \in \mathcal{V}} \alpha_{v,t} \cdot A_v^{val} \quad \forall t \in \mathcal{T} \qquad \text{Eq. 53}$$

Note that in the case of reactor area, additional McCormick relaxation constraints must be implemented to correctly constrain A_t', which is the product of the continuous variable Ω^R and binary variable Λ_t:

$$A_t' \leq \Lambda_t \cdot \max_{v \in \mathcal{V}} A_v^{val} \quad \forall t \in \mathcal{T} \qquad \text{Eq. 54}$$

$$A_t' \geq \Lambda_t \cdot \min_{v \in \mathcal{V}} A_v^{val} \quad \forall t \in \mathcal{T} \qquad \text{Eq. 55}$$

$$A_t' \leq \Omega^R - (1 - \Lambda_t) \cdot \min_{v \in \mathcal{V}} A_v^{val} \quad \forall t \in \mathcal{T} \qquad \text{Eq. 56}$$

$$A_t' \geq \Omega^R - (1 - \Lambda_t) \cdot \max_{v \in \mathcal{V}} A_v^{val} \quad \forall t \in \mathcal{T} \qquad \text{Eq. 57}$$

Three groups of constraints are needed to implement the power interpolation. First, the sum of weights of all the vertices must equal unity when the reactor is on and zero when it is off (Eq. 58). This constraint effectively restricts the weighting of the vertices to allow for interpolation between them.

$$\sum_{v \in \mathcal{V}} \alpha_{v,t} = \Lambda_t \quad \forall t \in \mathcal{T} \qquad \text{Eq. 58}$$

Second, if the reactor is on, only one simplex may be "active" at any time, meaning that the sum of all binary variables representing simplexes must also equal unity (Eq. 59).

$$\sum_{c \in \mathcal{C}} h_{c,t} = \Lambda_t \quad \forall t \in \mathcal{T} \qquad \text{Eq. 59}$$

Lastly, only vertices that are a part of the active simplex may have non-zero weights. To impose this constraint, we can bound the vertex weights by the sum of all simplexes that contain the given vertex (Eq. 60).

$$\alpha_{v,t} \leq \sum_{c \in M(v)} h_{c,t} \quad \forall t \in \mathcal{T}, \forall v \in \mathcal{V} \qquad \text{Eq. 60}$$

Where $M(v)$ is a function that maps every vertex to a set of simplexes that contain that vertex. The map is given as an input to the model along with vertex information, and is thus static during optimization.

For the model to accurately assess the costs of producing ammonia, the linearization must be able to estimate the power consumption accurately. The most straightforward way to increase the accuracy is to increase the number of linearization segments, i.e. increase the number of vertices and simplexes. However, with a larger number of interpolation segments, the model size and complexity increase, which increases the time necessary to find optimal solutions. For this reason, a balance between the size and accuracy of the model must be maintained. Ideally, an "optimal" set of vertices and simplexes should be used for any given function domain and target accuracy.

To appropriately select vertices and simplexes, we first started with a fine mesh representing the functional surface in the domain of interest (Fig. S4a). This fine mesh is considered to be a "true" representation of the functional surface. The domain of interest was usually defined by a minimum and maximum electrode area, a minimum and maximum production rate, and maximum obtainable current density (j_{max}), defined by the transport limited current density. The domain shape is typically not rectangular due to the specification of the maximum obtainable current density. The minimum production rate is meant to model the non-zero ammonia production rate necessary for the liquefication processes to function. The area and production rate were chosen to have a large range to allow for true optimization, yet the ranges were finite to restrict model size. The total area was ranged from 1000 to 30000 m^2, while the production rate ranged from the minimum allowable production rate (typically 50 kmol/hr) to 2500 kmol/hr. The minimum production rate was assumed to be non-zero as electrochemical systems often need to operate at a non-zero current density or can be shut down. Also, below a certain production rate of ammonia, the liquefaction ammonia separation method cannot work as not enough ammonia can be condensed out of the gas phase.

Once a fine mesh is made, it can be simplified through a mesh simplification algorithm that utilized quadratic error metrics (Fig. S4b).[55] Briefly, the algorithm iteratively merges pairs of vertices (and re-generates simplexes based on the new available vertices) based on the amount of

error (i.e. degree of simplification) that is introduced by performing the merge. A Python implementation of the algorithm, quad_mesh_simplify,[56] was used to generate the final meshes. Typically, a max_err=0.1 parameter value was used, which was found to give accurate results and reasonable model sizes. The resulting meshes sometimes contained vertices that were shifted from the original domain boundaries. For example, if one of the domain boundary points in the original, fine mesh was (1000 m^2, 50 kmol/hr), the simplified mesh might contain a point (1100 m^2, 55 kmol/hr). In these cases, the vertices closest to the domain-defining points were shifted back to the domain boundary. In the above example, the vertex at (1100 m^2, 55 kmol/hr) would once again become (1000 m^2, 50 kmol/hr), while other vertices would remain unchanged.

After the "optimal" vertices were found, the reactor power consumption for every vertex was recomputed using the vertex area and production rate; this was done to minimize the amount of error in the interpolated power consumption.

Computing reactor power consumption

The power consumption of the electrochemical reactor can be computed from the production rate of ammonia (x_t^{conv}) and the total electrode area Ω^R. The power consumption estimation was done outside of the MILP model, and only the vertices and simplices necessary for power estimation were fed into the model. Parameters used in power consumption estimation are defined in Table S4.

The power consumption is assumed to be a product of applied current, which can be computed from x_t^{conv}, and the potential across the reactor:

$$\Pi_t^R = V \cdot I = V \cdot j \cdot \Omega^R$$

The potential is a function of the current density in an electrochemical cell, not the absolute current, so the current density must be found. The production rate of ammonia and the current density in an electrochemical cell are related as follows:

$$x_t^{conv} = \frac{j\Omega^R}{3F_{scale}}$$

The potential (V_t) across the reactor can be assumed to consist of thermodynamic, overpotential, and resistive terms, where the overpotential and resistive terms are functions of current density.

$$V = U_0 + \eta(j) + R_{res} \cdot j$$

By using the above expressions and defining $\alpha = 3F_{scale}$, the power consumption of the reactor can be computed in terms of ammonia production rate and total electrode area:

$$\Pi_t^R = V \cdot j \cdot \Omega^R = \alpha x_t^{conv} \cdot (U_0 + \eta(j) + R_{res} \cdot j)$$

The equilibrium potential is assumed to change with temperature according variation in the Gibbs free energy of ammonia formation (assuming 1 mole of ammonia is formed in the reaction expression):

$$U_0 = -\frac{1}{3F}(\Delta H - T\Delta S)$$

The overpotentials can be assumed to consist of two kinetic overpotentials (one at the cathode, one at the anode), and two transport overpotentials:

$$\eta(j) = \eta_{kin,and} + \eta_{kin,cat} + \eta_{trans,and} + \eta_{trans,cat}$$

For simplicity, we will assume that the transport overpotentials at each electrode are equal:

$$\eta_{trans,and} = \eta_{trans,cat}$$

Typically, transport overpotentials are quite small up to the point the reaction is transport limited. For this reason, we may assume that the transport overpotential is defined by the more-easily limited reaction, as the value of either overpotential is likely to be small. The expression for transport overpotential, assuming a first order reaction at the electrode in the limiting species, is:

$$\eta_{trans,and} = \eta_{trans,cat} = \frac{RT}{3F}\ln\left(1 - \frac{j}{j_{max}}\right)$$

Assuming Butler-Volmer kinetics, the kinetic overpotential for the cathode (and analogously for the anode) is given by:

$$\eta_{kin,cat} = \operatorname{arcsinh}\left(\frac{j}{2i_{0,cat}}\right)\left(\frac{RT}{\alpha_{k,cat}F}\right)$$

Thus, the overpotentials can be computed in a closed form:

$$\eta(j) = \operatorname{arcsinh}\left(\frac{j}{2i_{0,cat}}\right)\left(\frac{RT}{\alpha_{k,cat}F}\right) + \operatorname{arcsinh}\left(\frac{j}{2i_{0,and}}\right)\left(\frac{RT}{\alpha_{k,and}F}\right) + \frac{2RT}{3F}\ln\left(1 - \frac{j}{j_{max}}\right)$$

The exchange current densities are assumed to change with temperature according to the Arrhenius equation (expressions for the cathode and anode are analogous):

$$i_{0,cat} = i_{0,cat}^{298} \cdot \exp\left(\frac{E_a^{cat}}{R} \cdot \left(\frac{1}{298} - \frac{1}{T}\right)\right)$$

The surface-scaled resistance of the electrolyte is a function of the electrolyte thickness, which is a varied parameter, and the conductivity of the electrolyte:

$$R_{res} = d_{elec} \cdot \frac{1}{\omega_0}$$

The resistivity of the electrolyte is also assumed to change with temperature according to an Arrhenius-like expression, though with a weak temperature dependence in an attempt to mimic the properties of Nafion:[57]

$$\omega_0 = \omega_0^{298} \cdot \exp\left(\frac{E_a^{res}}{R} \cdot \left(\frac{1}{298} - \frac{1}{T}\right)\right)$$

Assumptions regarding activation energies for all the terms were made and can be found in Table S4.

Table S4. Thermodynamic, kinetic, and transport parameter values used for reactor power consumption estimation.

Parameter	Value	Units	Description
R	8.314	J/(mol K)	Universal gas constant
T	-	K	Temperature of the reactor, which is a varied parameter
Π_t^R	-	W	Power consumption of the reactor, which is fed into the MILP model
V	-	V	Potential across electrochemical cells
I	-	A	Total current in through all the cells
j	-	mA/cm^2	Current density through the cells in the reactor

Ω^R	-	m^2	Total reactor area, which is fed into the MILP model
F_{scale}	2680	mA m^2 hr/(cm^2 kmol)	Faraday's constant, in appropriate units for the model
F	96500	C/mol	Faraday's constant in SI units
U_0	-	V	Equilibrium potential of the electrochemical reaction – varies with temperature
ΔH	-45940	J/mol	Enthalpy change in the reaction of N_2 and H_2 to form NH_3
ΔS	-99.1	J/(mol K)	Entropy change in the reaction of N_2 and H_2 to form NH_3
$\eta(j)$	-	V	Total overpotential in the electrochemical cells as a function of current density
$\eta_{x,y}$	-	V	Type of overpotential $x \in \{kin, trans\}$ (kinetic or transport) at electrode $y \in \{cat, and\}$ (cathode or anode)
j_{max}	-	mA/cm^2	Transport-limited current density, which is a varied parameter
$i_{0,cat}^{298}$	1	A/cm^2	Exchange current density of the anode reaction at 298 K
$i_{0,and}^{298}$	-	A/cm^2	Exchange current density of the cathode reaction at 298 K, which is a varied parameter
E_a^{and}	50000	J/mol	Energy of activation of the anode reaction to compute changes in exchange current density
E_a^{cat}	40000	J/mol	Energy of activation of the cathode reaction to compute changes in exchange current density
$\alpha_{k,and}$	0.5	-	Charge transfer coefficient of the anode reaction
$\alpha_{k,and}$	0.5	-	Charge transfer coefficient of the cathode reaction
R_{res}	-	Ohm m^2	Surface-scaled resistance of the electrolyte, which varies with the electrolyte thickness
d_{elec}	-	m	Thickness of the electrolyte, which is a varied parameter
ω_0^{298}	0.1	S/cm	Conductivity of the electrolyte at 298 K[58]
E_a^{res}	2000	J/mol	Effective energy of activation to predict electrolyte conductivity change with temperature, assumed to mimic Nafion properties[57]

Reactor capital costs

The capital cost of the stacks in the electrochemical reactor was assumed to be proportional to the total electrode area (Eq. 49). In order to estimate the cost of the scaling factor, we derived an expression for the per unit area cost of the reactor from the ground up. The process for this derivation is derived below.

The cost of the stacks typically scales linearly with the total area of the electrochemical reaction, as the reactor is scaled by increasing the number of stacks, not their size.

$$C_{stacks} = p^{A,R} \cdot \Omega^R = \frac{\Omega^R}{A_{stack}} \cdot C_{stack}$$

The cost of a single stack is a combination of several factors, including the cost of the separator (and electrolyte), the electrodes, and the catalysts. Each stack also needs backplates to carry current, gases, and act as heat exchangers, the cost of which is proportional to the area of a single cell, and a frame to compartmentalize the stack. A single cell is assumed to have an area of 600 cm^2, and 100 cells are assumed to be in every stack. These values are similar to those used in large-scale water electrolyzers.[42]

$$C_{stack} = A_{stack} \cdot (C_{mem} + 2C_{elec} + C_{cat} \cdot m_{cat}) + f_{oversize} \cdot A_{cell} \cdot C_{BP} + C_{frame}$$

Estimated values of the capital cost parameters can be found in Table S5.

Table S5. Values of parameters related to electrochemical reactor cost estimation.

Parameter	Value	Units	Description
A_{stack}	6	m^2	Total area of all cells in the stack
A_{cell}	0.06	m^2	Area of a single cell of in the stack
C_{mem}	1000	\$ m^{-2}	Cost of membrane per unit area
C_{elec}	500	\$ m^{-2}	Cost of electrode material
C_{cat}	0.07	\$ mg^{-1}	Cost of catalyst material (~cost of Pt)
m_{cat}	10000	mg m^{-2}	Catalyst loading
$f_{oversize}$	2		Backplate oversizing factor
C_{BP}	10000	\$ m^{-2}	Cost of backplates at ends of a stack
C_{frame}	100	\$	Cost of assembly frame for a stack
C_{power}	220	\$ kW^{-1}	Cost of power supplies
f_{eff}	2	-	Factor to account for cooling inefficiencies

Supplementary Discussion

Choice of unit operations

As with all chemicals manufacturing processes, implementing the electrochemical synthesis of ammonia using air, water, and renewable electricity as feedstocks will require several unit operations in addition to the chemical reaction unit. These auxiliary unit operations, such as feedstock purification, product separation, etc. may in principle be realized with many different technical approaches, each with several different technical parameters of their own. Since our study focuses on formulating key technical goals for the electrochemical reaction unit, and to avoid a factorial complexity of analysis, we narrow the scope of our study to consider only the most economically viable methods for realizing the auxiliary unit operations, based on their process cost and technical maturity. Here, we describe the technoeconomic considerations that informed our choices to restrict the model to consider only a particular implementation of a certain unit operation.

While electrochemical ammonia production could in theory utilize ambient air as a nitrogen source,[35,59] this nitrogen may instead be selectively purified in a unit operation prior to the electrochemical reaction. Purification can remove possible catalyst poisoning agents (O_2, CO_2) and achieve the highest selectivity towards ammonia production. Air separation technologies are mature, inexpensive, and are relatively energy efficient,[60] with pressure-swing adsorption (PSA) systems consuming as little as 0.11 MWh per ton N_2 produced from air.[43] Hence, our model assumes that the air feedstock must be separated to produce a pure nitrogen feed to the reactor. While cryogenic distillation units can produce large volumes of nitrogen at high purity, they cannot be scaled down cost-competitively, and suffer poor utilization of intermittent energy resources.[60] In our TEA, we assume that the air purification step is carried out by pressure-swing PSA units, which produce extremely pure nitrogen (>99.99%),[43] can be operated in a modular fashion, and are robust to intermittency in the power supply. In the model, the PSA units were assumed to produce pure nitrogen to simplify mass balances. Membrane separation systems have been discussed as an alternative to PSA units; while they are modular and deployable at the scales considered here, they do not typically produce nitrogen at the same purity as PSA units.[61]

The hydrogen incorporated into the ammonia must ultimately be sourced from water, either through pre-electrolysis of water to produce a pure hydrogen feed stream, or through direct nitrogen reduction in water. Direct nitrogen reduction with water seems initially appealing because it removes a unit operation (water electrolysis), resulting in an intensified process with fewer capital-intensive pieces of equipment. Yet, this approach faces a couple important drawbacks. First, nitrogen reduction in nonaqueous media is preferred, as it improves the selectivity for ammonia by reducing the rate of hydrogen evolution as compared to an equivalent reaction in aqueous media.[23] However, water oxidation, the counter-reaction at the anode, is kinetically difficult and energetically inefficient in nonaqueous electrolytes due to reduced thermodynamic water activity and likely reduced kinetic catalyst activity, whereas hydrogen oxidation has been demonstrated robustly in nonaqueous media, especially when using solvent-agnostic gas diffusion electrodes.[13] Second, water electrolysis methods are sophisticated and well-studied due to significant research and industrial interest in building a hydrogen economy,[62] which suggests that approaches utilizing water electrolysis may be more mature than those utilizing direct water oxidation-coupled nitrogen reduction. Several electrolyzer technologies, such as alkaline electrolysis, proton exchange membrane (PEM) electrolysis, anion exchange membrane (AEM)

electrolysis can produce hydrogen in a highly optimized manner. Given these considerations, our analysis assumes that electrochemical nitrogen reduction is achieved using hydrogen feedstock produced from water using a PEM electrolysis unit, which can produce hydrogen at pressures up to 30 bar, has fast response times and detailed future cost estimates.[42,63] The electricity consumption for hydrogen production is assumed to be constant with respective to production rate and equal to 47.6 MWh/ton H_2.

Many different methods of producing ammonia from nitrogen, hydrogen, and renewable energy have been discussed, which can be broadly categorized into low-temperature electrochemical, high-temperature electrochemical, and plasma-based techniques. We rule out plasma-based approaches in our analysis due to concerns related to energy efficiency[64,65] and low single-pass conversions compared to electrochemical methods.[8] Similarly, we rule out high-temperature approaches in the present analysis. Thermodynamically, nitrogen reduction to form ammonia is unfavored at high temperatures (Fig. S2), often resulting in a lower single-pass conversion at an equivalent applied potential.[66] Additionally, there is risk of ammonia decomposition at higher temperatures further from the electrode, where the effects of potential are not as significant. High temperature operations may also introduce greater thermal inertia into a process, increasing capital costs associated with effecting rapid changes in gas stream temperatures, as well as compromising process flexibility in response to renewable power intermittency. As low-temperature (<100 °C) nitrogen reduction approaches have shown significant promise under laboratory conditions, achieving single-pass conversions of >80% at near-ambient operating conditions,[13] we restrict our analysis to this technology.

Finally, the ammonia in the effluent stream from the electrochemical reactor must be separated from the unreacted nitrogen and co-produced hydrogen and any electrolyte. In our analysis, we assume that the ammonia can be found predominantly in the gas phase; produced ammonia will tend to accumulate in the gas phase when the electrolyte is saturated with ammonia during steady state operation. We assume that the ammonia will be separated in a manner similar to the Haber-Bosch separation process, using a liquefaction unit that is well suited to separating inlet streams at high ammonia concentrations. While alternative methods for separating ammonia exist, such as adsorption by metal salts,[67] they are often more capitally intensive and are usually employed for inlet streams with low ammonia partial pressures for which liquefication is not viable.[43] As the partial pressure of ammonia in the product stream is high when using electrochemical processes, the more-established and less capitally-intensive liquefication option can be used.

Effect of electricity source

Broadly, if a single source of power is used, the ammonia cost correlates well with the levelized cost of electricity (LCOE), an often-cited quantitative metric that incorporates the power availability and the cost of installing new renewable energy resources (Fig. 2a, b). If multiple power sources can be used for power generation, such as PV and wind, then the relationship between the effective combined LCOE, which is computed from the costs and generation of each power source in proportion to their capacity, and ammonia production cost is not as clear (Fig. 2c). However, across the 50 locations investigated, the predicted ammonia cost is always lower when both PV and wind generation are used instead of any single power source. Mixing two different power sources with non-overlapping intermittency schedules results in a greater average power availability, as one power source can "fill in" during periods of low generation for the other source

(Fig. S1). Increased power availability in turn allows the plant to operate at lower production rates for more time to meet a fixed output requirement, resulting in a lower implied peak production rate.

Effect of Faradaic efficiency

First, we examined the effect of changing the Faradaic efficiency toward NH_3 in the electrochemical reactor on the cost of produced ammonia. We find that when deviating from the generally efficient (0.8 V overpotential) base case, the cost of ammonia is weakly inversely correlated with Faradaic efficiency (Fig. S6). The two main contributors to the changes in NH_3 costs were the capital costs of VRE and the cost of the nitrogen reduction reactor. As the Faradaic efficiency decreases, a larger fraction of the current in the ammonia synthesis reactor goes towards producing the side product hydrogen, which needs to be recycled. This increases the total amount of energy that must be expended to produce ammonia (Fig. S6), necessitating larger amounts of VRE installations to supply the energy. With increased amounts of gas reactant recycling, the reactor size is also increased. Most other cost contributors do not change significantly with Faradaic efficiency. For an inefficient ammonia production reactor, however, a significant source of cost is increased requirements for energy storage (Fig. S7, Fig. S8).

Effect of reactor temperature

The operating temperature of the reactor can affect both the efficiency of the reactor as well as general plant operation. Increased temperatures can increase the exchange current densities of reactions occurring at the electrodes, thereby lowering the overpotentials of the electrode reactions, thus increasing energy efficiency. The rates of ammonia synthesis and hydrogen evolution may increase to different extents with temperature, leading to a change in the Faradaic efficiency to ammonia. As these changes are chemistry specific, they cannot be assessed in the present, black-box chemistry modeling approach. Additionally, temperature increases can lower the resistivity of the electrolyte, further decreasing energy consumption in the reactor. On the other hand, a higher operating temperature necessitates more cooling of gases prior to NH_3 liquefication and more heating prior to entering the cell; these additional energy uses may or may not outweigh the energy savings associated with a more efficient electrochemical reactor. At high temperatures (>150 °C) and moderate pressures, ammonia dissociation into nitrogen and hydrogen could become an issue, lowering the conversions (Fig. S2) and effective Faradaic efficiencies obtainable. We found that, with the current assumptions, changing the temperature of the reactor in the 30-90 °C range does not significantly change the cost of ammonia, though the energy consumption (i.e. VRE capacity) and size of the reactor are decreased somewhat (Fig. S13).

Development of efficiency metrics and analysis thereof

We sought to apply our model towards understanding key operating parameter groupings that can predict the final cost of fully electric ammonia production in order to outline key targets for the technical viability of an electrochemical ammonia synthesis process. Parameter groupings that are well-correlated with the final production cost of ammonia can inform important rules of thumb for guiding the development of new nitrogen reduction technologies at the lab and pilot plant scale. We used the model to explore the system dynamics, ammonia synthesis cost, and performance requirements to achieve cost parity with both conventional fossil-fuel based ammonia

production ($0.4-0.7/kg) and electrolytic hydrogen- coupled with Haber-Bosch based ammonia ($0.8-1.0/kg).[28] The flexible, fully electrochemical approach utilized little high-cost battery and hydrogen storage, instead utilizing inexpensive ammonia storage to counter the intermittent nature of renewable electricity generation.

The final cost of ammonia can be grouped broadly into three groups: energy consumption-related (VRE and energy storage) capital costs, reactor capital and operating costs, and separations capital and operating costs. The water electrolysis, ammonia liquefaction, and air separation units are mostly unaffected by changes in the operating parameters of the chemical reactor or contribute little to the final ammonia cost (Fig. 2d, Fig. S6). In total, these units consistently contribute 0.2-0.25 $/kg to the final cost of ammonia when both PV and wind can be used as power sources; the contribution is higher when a single power source is used (Fig. 2d). Hence, we seek technical metrics that can predict the energy production capital costs and the capital cost of the electrochemical reactor, as these are the most affected by the chemistry and are therefore crucial for assessing the viability of an electrochemical ammonia synthesis process.

Changes in the total energy consumption of the ammonia production plant are dominated by the ammonia synthesis reactor (Fig. S6). The changes in energy consumption of the electrochemical reactor implicitly bundles the effects of Faradaic efficiency, kinetic overpotential, applied current density, and cell resistance in a complex function form. An alternative, simpler metric that is often quoted in the nitrogen reduction literature is the effective energy efficiency of the electrochemical reactor.[13,16,29] One source of energy loss is the production of hydrogen, which is a side product; the effect of this loss can be captured in the Faradaic efficiency. A second loss is associated with overpotentials in the reactor. Considering these two losses, the energy efficiency can be described by:

$$EE_R = FE_{NH_3} \cdot \frac{V_{NH_3,ideal}}{V_{NH_3,ideal} + \eta_R}$$

Where $V_{NH_3,ideal}$ is a free-energy based potential for ammonia synthesis from air and water, assumed to be 1.18 V, and η_R is the overpotential in the reactor. Energy storage can allay the inherent intermittency of VRE, allowing the plant to produce ammonia at a lower rate for a longer span of time in order to meet a fixed total ammonia production rate. Given the necessity of energy storage, especially for energy-intensive ammonia production, we include the cost of energy storage in the total cost of energy when making the cost-efficiency correlation.

This energy efficiency can be correlated to the total cost of energy generation and storage in the plant (Fig 6a). We find that at low energy efficiencies (<30%), the cost of energy necessary for the plant increases dramatically with losses in efficiency. At higher energy efficiencies, however, the cost of energy appears to be relatively constant with energy efficiency, thus pointing to the difficulty of further reducing energy and ammonia costs with improvements in energy efficiency. Based on the lower bound of energy cost at a given energy efficiency and the definition for energy efficiency above, we can compute the maximum allowable overpotential given a reaction overpotential and desired energy cost (Fig. 4c). As the goal of this work is to define minimum productivity metrics necessary for making fully electrochemical ammonia production viable, we decided that an energy cost of 0.6 $ kg^{-1} is necessary for viable ammonia production, keeping in mind all assumptions described in the Methodology. Lower energy costs are more difficult to achieve and require significantly more efficient chemistries, while higher costs may make fully electrically-produced ammonia economically less viable.

For the energy costs to be ≤0.6 $ kg^{-1}, the energy efficiency of the ammonia production reaction must be ≥32% (Fig. 4c). In order to achieve this energy efficiency, the Faradaic efficiency

toward ammonia must be at least 32%, assuming that there is no overpotential at either electrode for producing ammonia. This result implies that many reported chemistries utilizing aqueous electrolytes, while claiming low overpotentials,[30–32] cannot be used for economically viable fully electrochemical ammonia production due to low FEs alone. At unity (100%) Faradaic efficiencies, the overpotential of the reaction must be ≤2.45 V to maintain energy efficiencies ≥32%. This finding implies that lithium-mediated nitrogen reduction which often reports of overpotentials in excess of 3 V,[7,13,20,33,34] also requires fundamental modifications to decrease the overpotential for economic viability of the chemistry.

While the simple definition of energy efficiency as described above can be correlated to the energy cost for producing ammonia relatively well, it does not capture other sources of energy loss, such as losses due to resistive heating and separations, as well as the need for compound recycling; some of the spread in predicted costs at single values of energy efficiency can be attributed to this. For this reason, it makes sense to propose alternative energy efficiency metrics that may be able to predict energy costs with less uncertainty. An example of modified energy efficiency which appears to more accurately predict energy costs (Fig. S15) is described in the Supplementary Discussion.

The capital cost of the electrochemical ammonia synthesis reactor is a more complex function that depends on several parameters, such as desired peak production rate and maximum current density of the ammonia production reactor. In the absence of energy input variation and energy losses, the optimal strategy is likely to operate as close as possible to the maximum possible current density to maximize production and minimize reactor size. For this reason, we attempted to correlate the capital cost of the electrochemical reactor with the product of the maximum obtainable current density and Faradaic efficiency, i.e. the maximum partial current density for ammonia production (Fig. 4b). We found that the metric can give a lower bound for the capital cost of ammonia synthesis reactor. If the reactor experiences a large amount of resistive losses at high current densities, the optimum operating current density may be lower than the maximum possible one. This implies that a resistive electrolyte would increase the necessary reactor size and total capital cost, which may explain the observed spread in reactor capital costs (Fig. 4b). At partial current densities above ~400 mA cm^{-2}, the capital cost of the reactor does not change as significantly as at lower production rates (Fig. 4b, d) and reaches a value of 0.1-0.2 \$ kg^{-1}. In light of this, we suggest that an approximately 400 mA cm^{-2} ammonia partial current density is likely necessary for economic viability of electrochemical ammonia production. This partial current density can be achieved by increasing the total current density, the Faradaic efficiency to ammonia, or both. At the moment, no nitrogen reduction chemistry has reported production rates of this magnitude, though approaches for increasing rates through pressurization and the use of high surface area electrodes,[68] as well as the use of gas diffusion electrodes[13] have been reported. This suggests that breakthrough improvements to the electrolyte and chemistry are critical for the lithium-mediated nitrogen reduction approach to be economically viable for large-scale centralized ammonia production using renewable resources.

Taken together, the cost of ammonia for a system that reaches above mentioned minimum viable production metrics can approach 0.9-1.0 \$ kg^{-1} when using both PV and wind power in West Texas. These costs are competitive with a 2nd generation, semi-electrochemical ammonia synthesis methods.[4] When using renewable power source with lower capacity factors, the production metric will likely need to improved further to stay competitive with other ammonia synthesis methods. In addition, an implicit assumption regarding the stability of the chemistry was made when computing the capital cost of the electrochemical reactor. The plant lifetime is assumed

to be 20 years, and the capital cost of the reactor is annualized over the entire period. If the electrochemical reactor requires often replacement of electrolyte, catalyst, or of other components, then the capital costs would go up proportionately, and higher ammonia partial current densities would be required for low-cost ammonia. The lifetime of the reaction is important to consider in electrochemical nitrogen reduction, as few reports report operation for longer than a few hours,[13,16,35,36] and practically no reports exist for continuous ammonia production for over hundreds of hours. In addition to improving the partial current density and energy efficiency toward ammonia synthesis, significantly improvements must be made to the lifetime of the process for economic viability of fully electrochemical nitrogen reduction.

Effect of plant-wide parameters

Certain operating parameters of the electrochemical reactor affect not only the efficiency of the electrochemical reaction, but also other parts of the plant in a coupled fashion. Two examples of such parameters are the operating pressure of the electrochemical cell and the minimum required production rate. We examined the effects of these two parameters on the costs of NH_3 and found that certain values of these parameters are undesirable in a practical system.

The pressure in the electrochemical ammonia synthesis reactor affects many parts of the overall process. Increased pressure in a thermochemical process is used to affect the equilibrium of the ammonia synthesis reactor to increase conversion (Fig. S2). In an electrochemical system, especially one operating at low temperatures, the equilibrium is often shifted toward ammonia due to the application of potential even with a lack of pressurization. Increased pressure may increase the rate of the reaction at a constant potential by affecting the exchange current density. However, if the exchange current density is first order with respect to partial pressure of the reactants, then the change in potential is on the order of tens of millivolts for an order of magnitude increase in system pressure. In case of large potentials (>1 V) that may be present in the system from other losses, the pressurization of the reactor decreases the energy consumption of the reactor by only several percent. However, if pressurization can improve the selectivity toward ammonia, as has been reported for lithium-mediated nitrogen reduction,[16] then pressurization could be desirable. However, such effects are chemistry specific, and are thus outside the scope of this work. On the other hand, the gases must be pressurized before entering the cell, which may incur additional energy costs. Luckily, the air separation unit, water electrolysis unit, and N_2 and H_2 storage all operate at pressure of 30 bar or higher, so a reactor pressure of 30 bar or lower can be maintained without additional energy costs. A pressurized reactor will likely have higher capital costs, particularly in the design of the stack casing, gas manifolds, and backplates. As these parts are not the largest cost contributors to the cost of the reactor, the cost of the reactor may not change significantly at moderate (<30 bar) pressures.

The primary role of pressure in the system is to aid the liquefaction of the NH_3 when separating it from other gases leaving the reactor. Higher pressure reduces the fraction of ammonia in the gas phase in the liquefaction process, thereby improving separations. While lowering the liquefaction temperature can also improve separations, lowering it below -30 °C may require a different refrigeration system, which would increase capital costs for separations. For this reason, the flash tank temperature in the separation unit was kept constant at -30 °C. At this liquefaction temperature, we find that the reactor pressure does not significantly affect the cost of ammonia for reactor pressures above 5 bar (Fig. S12). For pressures below 5 bar, the ammonia separations are not efficient enough and require a slight scale-up of both the separations and ammonia

electrochemical reaction. At 2 bar and below, the costs are increased significantly. We are not accounting for changes in capital costs necessary for pressure increases, as well as potential kinetic losses due to having a large concentration of ammonia at the anode due to poor separations. In light of this, a reactor pressure of at least 5 bar is likely necessary for economically viable ammonia production. However, the reactor pressure likely should be below 30 bar to avoid high costs associated with high-pressure operation.

Electrochemical processes, particularly water electrolysis, while being flexible, typically have a lower bound on the production rate at which they can operate or must be shut down. In the case of water electrolysis, this is due to the possibility of hydrogen cross-over from the cathode to the anode at low current densities, which is a productivity, purity, and safety concern. For this reason, water electrolyzers typically operate at current densities above 10% of their maximum capability.[69] While it is not clear whether an electrochemical ammonia producing system would have similar issues, it is important to assess the impact of potential inflexibility of the plant. Other parts of the plant could also impose limitations on the minimum production rate of ammonia; for instance, the liquefication process may not be able to condense ammonia in a fixed-size flash tank if the ammonia content is too low due to the low production rates.

We varied the lower bound for the ammonia production rate while keeping the maximum current density constant at 1000 mA cm^{-2} by changing the shape of the allowable rate-area space (Fig. S4). The minimum production rate was found to have only a minor effect on ammonia costs (Fig. S14). While the flexibility of the plant is technically reduced, it does not typically have a significant impact as the system typically operates at the maximum production rate for a majority of the time, as this increases the utilization of capital resources.

When both PV and wind were used as power sources, the costs increase only when the minimum production rate was set to be above ~600 kmol hr^{-1} (10.5 ton hr^{-1} or nearly equal the nameplate plant capacity of 250 ton day^{-1}). Typically, a plant utilizing both PV and wind attempts to operate at a large range of high production rates, with a large fraction of production occurring at peak power availability (Fig. S14). If the minimum production rate exceeds the optimized productivity of ~10 ton hr^{-1}, then the plant must be optimized more for peak production, which increases costs.

On the other hand, when only PV was used as a source of energy, the minimum production rate had practically no effect on final NH_3 costs regardless of magnitude, though the optimal system behavior changed: less energy storage was used, while the size of units relevant to ammonia synthesis and separation increased (Fig. S14). These features can be explained by looking at the distribution of production rates when using PV only. In these cases, ammonia is typically produced at high rates during peak availability, or at low rates using stored power; this strategy allows for smaller reactor sizes due to larger utilization factors for the reactor. If the low rates are disallowed, then storage becomes unnecessary, while the reactor size must be increased. However, as these effects are balanced, increases in ammonia costs are avoided.

Alternative energy efficiency metric

While the definition of energy efficiency described in the main text is sufficient to predict the capital cost of VRE capacity and energy storage in a fully electrochemical ammonia production plant, the metric is not quite rigorous as it does not fully capture interacting plant parts. Therefore, we sought to modify the energy efficiency metric to better capture these effects.

The energy consumption of the entire plant can be written as a sum of the energy consumptions of all parts of the plant:

$$E_{total} = \sum_{u} E_u$$

We can assume that every unit operation has an "energy efficiency", which can be thought of a loss at each step. Ideally, these energy efficiencies should be multiplicative, where the total energy efficiency is a product of unit energy efficiencies:

$$\phi_{total} = \prod_{u} \phi_u$$

Unfortunately, multiplicative energy efficiencies do not capture the realities of a multi-step process well, and are in conflict with additive energy consumptions above. However, in the case of ammonia synthesis, there are only two main consumers of energy, which allows some analysis to be performed with these definitions. The water electrolysis unit and the ammonia synthesis reactor are the two largest consumers of electricity in the process (Fig. S6). Therefore, we can write:

$$E_{total} = E_{WS} + E_R$$
$$\phi_{total} = \phi_{WS} \cdot \phi_R$$

The energy efficiency of the water splitting step can be written as follows:

$$\phi_{WS} = \frac{E_{H2,ideal}}{E_{WS}}$$

Where $E_{H_2,ideal}$ is free energy change required to produce hydrogen from water. In the present model, $\phi_{WS} \approx 0.7$.

The total energy efficiency of the entire ammonia production process is

$$\phi_{total} = \frac{E_{NH_3,ideal}}{E_{total}}$$

Where $E_{NH_3,ideal}$ is the free energy change required to produce ammonia from nitrogen and water. Rearranging the above expressions, we can find the energy efficiency of the reactor

$$\phi_R = \frac{E_{WS}}{E_{H_2,ideal}} \cdot \frac{E_{NH_3,ideal}}{E_{WS} + E_R} \qquad \text{Eq. 61}$$

This definition assumes that energy is only used to produce hydrogen and ammonia from it, i.e. all other unit operations do not utilize energy. This assumption is relatively accurate in the present system (Fig. S6), though other consumers of energy can be included in the expression for total energy consumption with minimal effect.

We believe that this modified energy efficiency can be used to predict the total cost of energy generation and storage in the plant with less uncertainty and more rigor than the simplified energy efficiency described in the main text (Fig. 4).

Supplementary Figures

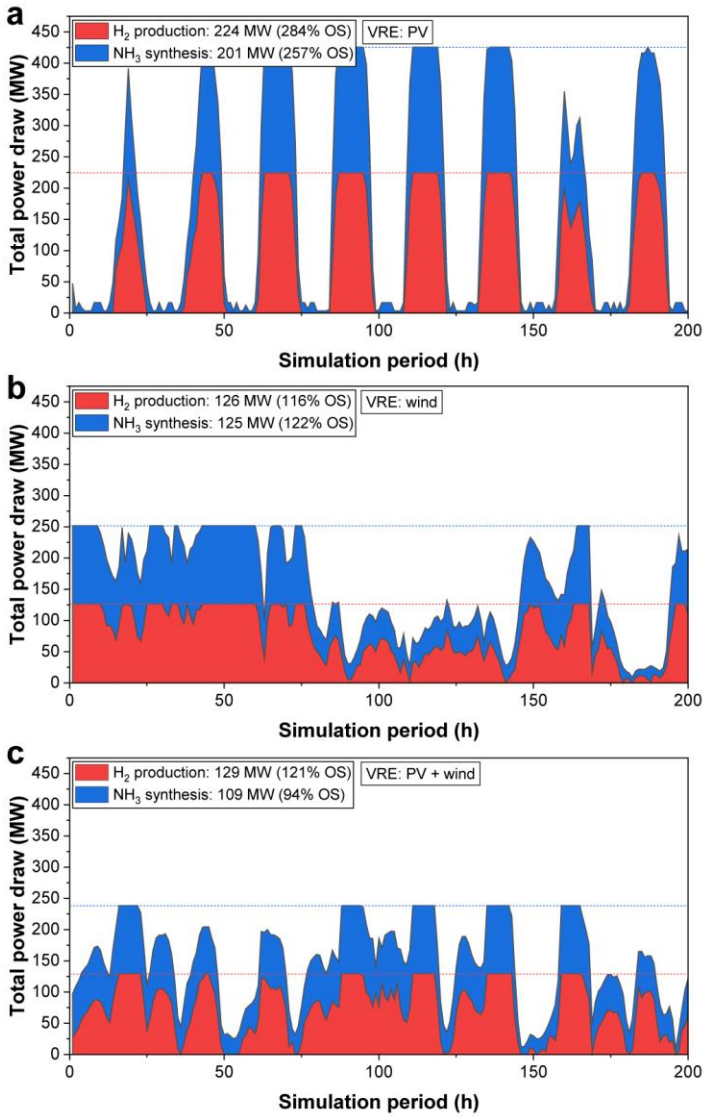

Fig. S1. The power consumption of the H_2 and NH_3 producing units, which utilize the majority of the power in the plant, when (a) only PV (b) only wind (c) both PV and wind in West Texas are used to generate electrical energy, using the base case model parameter values in Table 1. The maximum power consumptions of the water electrolyzer and ammonia synthesis reactor are reported in MW. The oversize fraction (OS) reported is defined to be the percent increase of the maximum power consumption of the unit relative to the minimum possible energy consumption (for a plant that continuously produces ammonia); effectively, the oversizing can be thought to be of an inverse of the capacity factor. In this case, the lowest possible continuous energy consumptions are 58 MW and 56 MW for the water splitter and ammonia synthesis reactor, respectively. The water electrolyzer and ammonia reactor in the PV-only case must be significantly oversized to accommodate the reduced capacity factors due to lack of power generation at night. Some ammonia can be produced from stored hydrogen and electricity at night even in a PV-only case. In other cases, the size of the electrolyzers and reactors can be smaller, lowering overall ammonia costs due to lower capital costs.

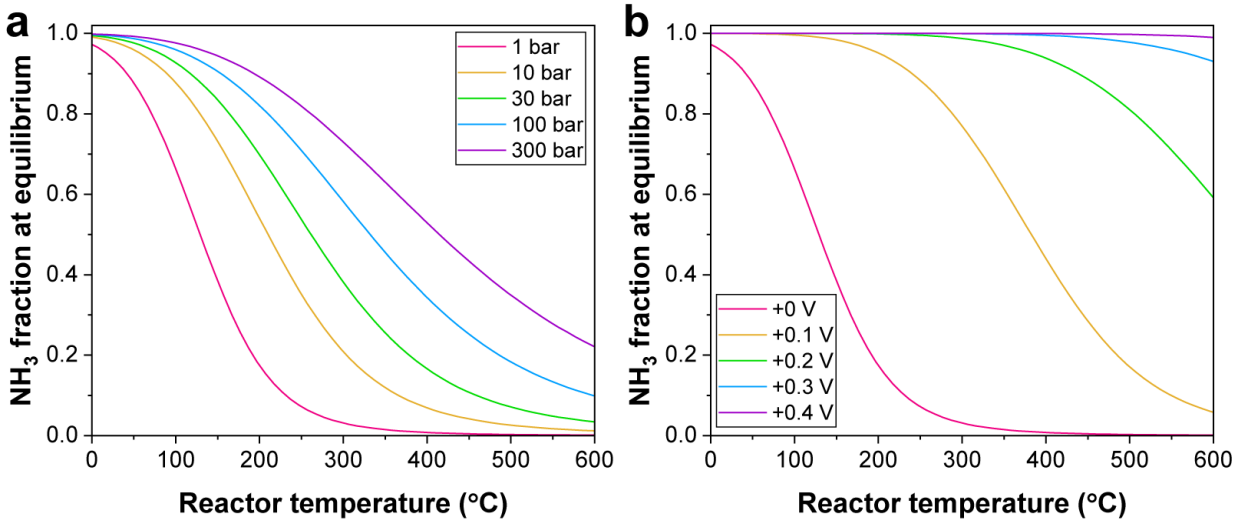

Fig. S2. Equilibrium conversion of ammonia for a 3:1 H_2:N_2 feed mixtures in reactors using (a) pressure and (b) electrochemical potential for driving equilibrium forward. Note the relatively low potential necessary in excess of the equilibrium potential to derive the reaction to completion.

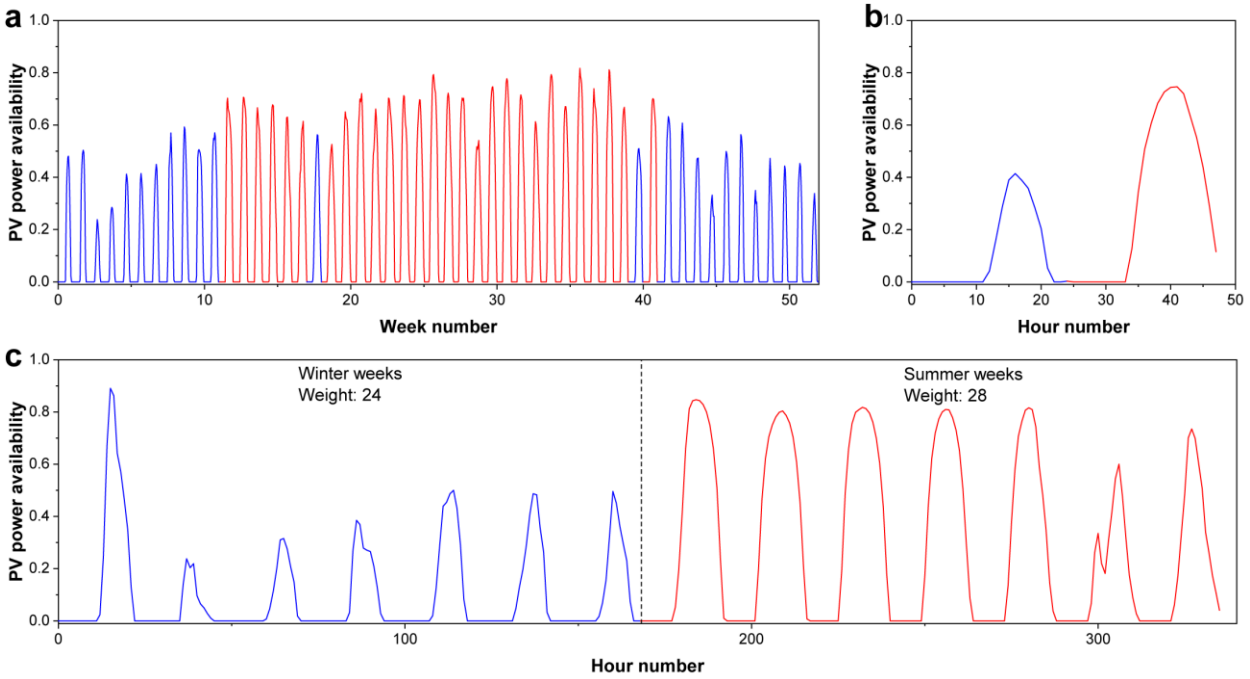

Fig. S3. Selection of representative weeks from PV availability data. (a) Weekly average PV availability across 24 hours of the day in NY. Each peak depicts the average of 7 days of PV availability for each of 24 hours. Depicting the hourly data for the entire year is difficult, which is why the weekly average is shown. Note that the peak availability increases during the summer weeks (weeks 20-40). The weeks are color coded based on their final attribution to winter (blue) or summer (red) weeks. (b) Weekly average PV availability from 2 representative weeks. Note how one week is a low PV availability week (blue, "winter"), and one is a high PV availability week (red, "summer"). The weighting of the weeks is non-uniform. (c) Hourly PV availability data for the two representative weeks. Note the hourly and daily changes in PV availability, and how they differ for winter and summer weeks. The data of the sort depicted in (c), with appropriate weights, was typically used to run the MILP model, with the difference that 6 representative periods were typically used, as opposed to only 2 as presented here.

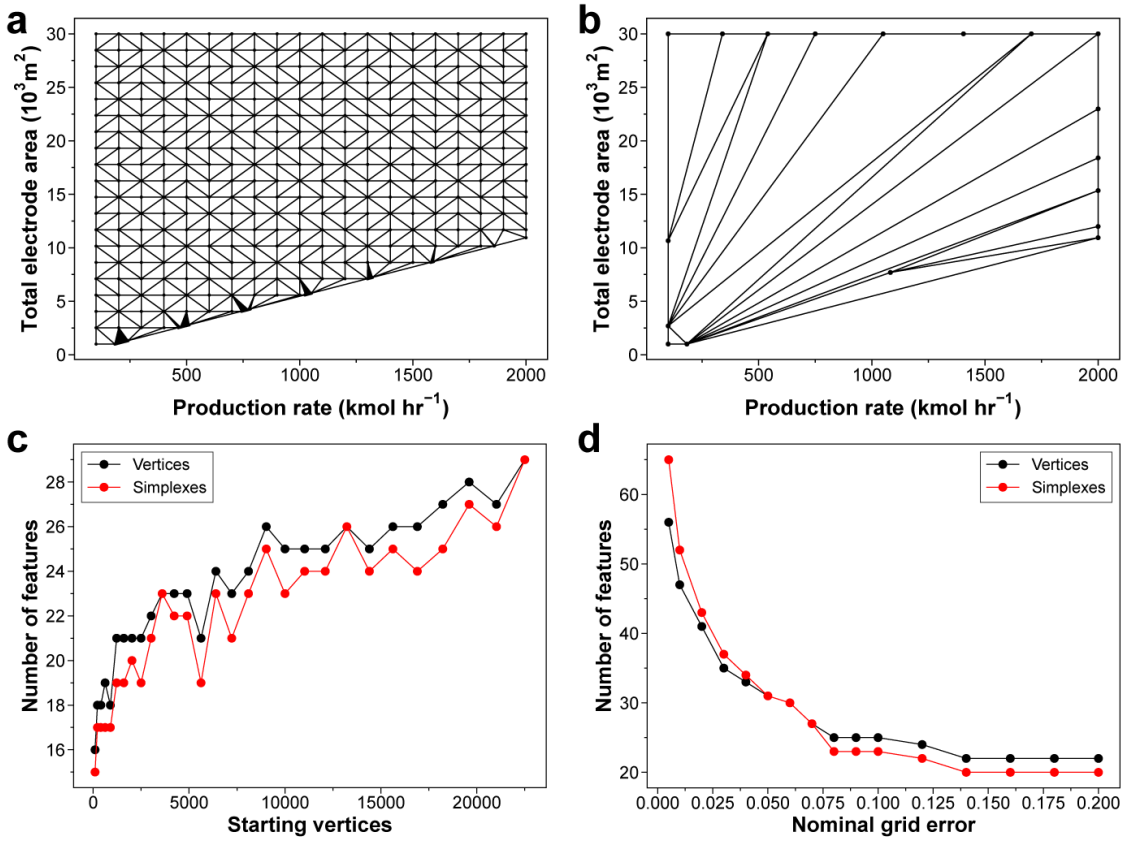

Fig. S4. Simplexes used to estimate the power consumption of the electrochemical reactor from the reactor area and NH_3 production rate. (a) An initial fine mesh of simplexes with ~350 vertices, which can be used in the MILP model to estimate the power consumption with high fidelity, yet with low computational cost. (b) A mesh produced from the mesh in (a) by merging simplexes using quadratic error metrics. A max_err=0.1 parameter value was used with a Python implementation of a mesh simplification algorithm.[56] These simplexes can still accurately predict the power consumption but utilize features of the form of the power consumption function to minimize the number of binary variables and lower computational cost. (c) The relationship between the number of vertices and simplexes necessary to represent a simplified mesh using a max_err=0.1 parameter value from a mesh with different numbers of starting points. The final mesh size is not a strong function of initial mesh size once more than ~2500 points are used for the initial mesh. (d) The relationship between the number of vertices and simplexes necessary to represent a mesh with a variable value of the max_err parameter, here labeled as "Nominal grid error". The starting mesh is composed of ~9000 points. As the nominal grid error decreases, a more detailed mesh is necessary, which may increase computational cost. A nominal grid error of 0.1 strikes a balance between model complexity and accuracy.

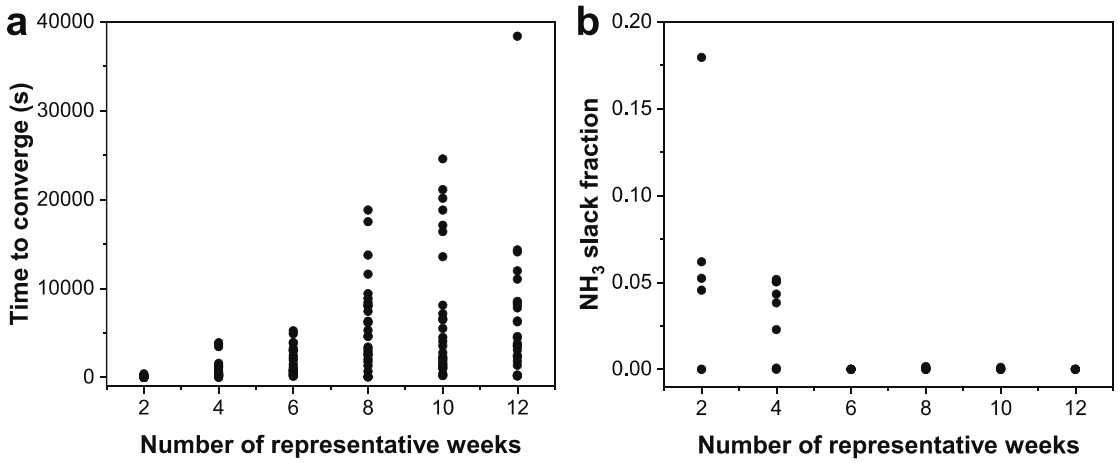

Fig. S5. Effect of the number of representative weeks used on MILP model conversion time and accuracy. The base-case parameters described in Table 1 were used for the simulations, except PV-only energy generation was used and FE was varied between 50 and 90%. (a) The effect of the number of representative weeks on time to converge the plant sizing model. While models of all sizes can converge rapidly, models with a larger number of weeks have higher average and upper bound convergence times. (b) The effect of the number of representative weeks used in sizing the plant on the fraction of ammonia that must be obtained using the slack variable in full-year simulations. With a sufficiently large number of representative weeks (here ~6 weeks), the slack fraction is close to zero, meaning the plants are appropriately sized. Reproduced from ref. 27, MIT 2021.

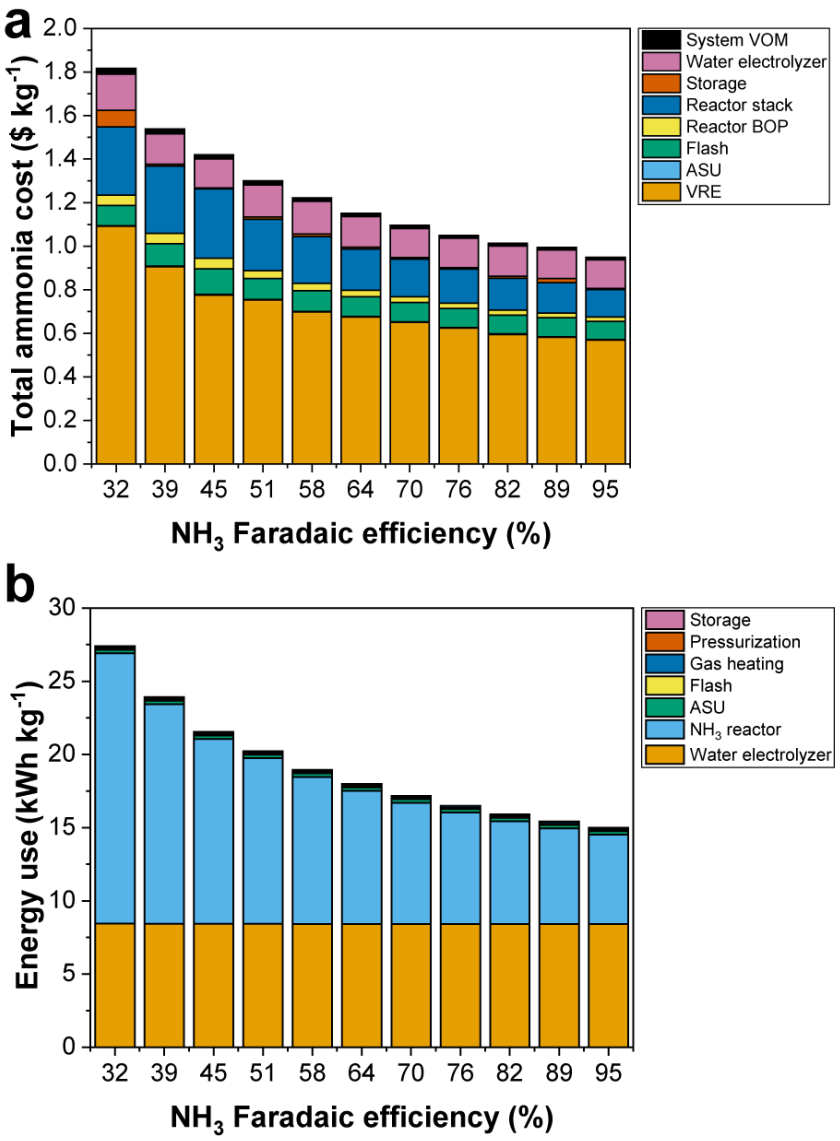

Fig. S6. The contributions of various parts of the ammonia plant on the price of ammonia as a function of reactor Faradaic efficiency for a reactor with moderate energy efficiency. All of the base case assumptions described in Table 1 were used in the analysis. The kinetic overpotential was assumed to be ~0.8 V, which is the overpotential used in the base case throughout the analysis. Both PV and wind in West Texas were used as possible power sources. At low Faradaic efficiencies, it is optimal to build a larger amount of battery storage; some ammonia, hydrogen, and nitrogen storage is built under all conditions, but their relative contributions to cost are low. Under most conditions, simply building more VRE capacity and a larger ammonia production reactor is optimal compared to building expensive battery storage.

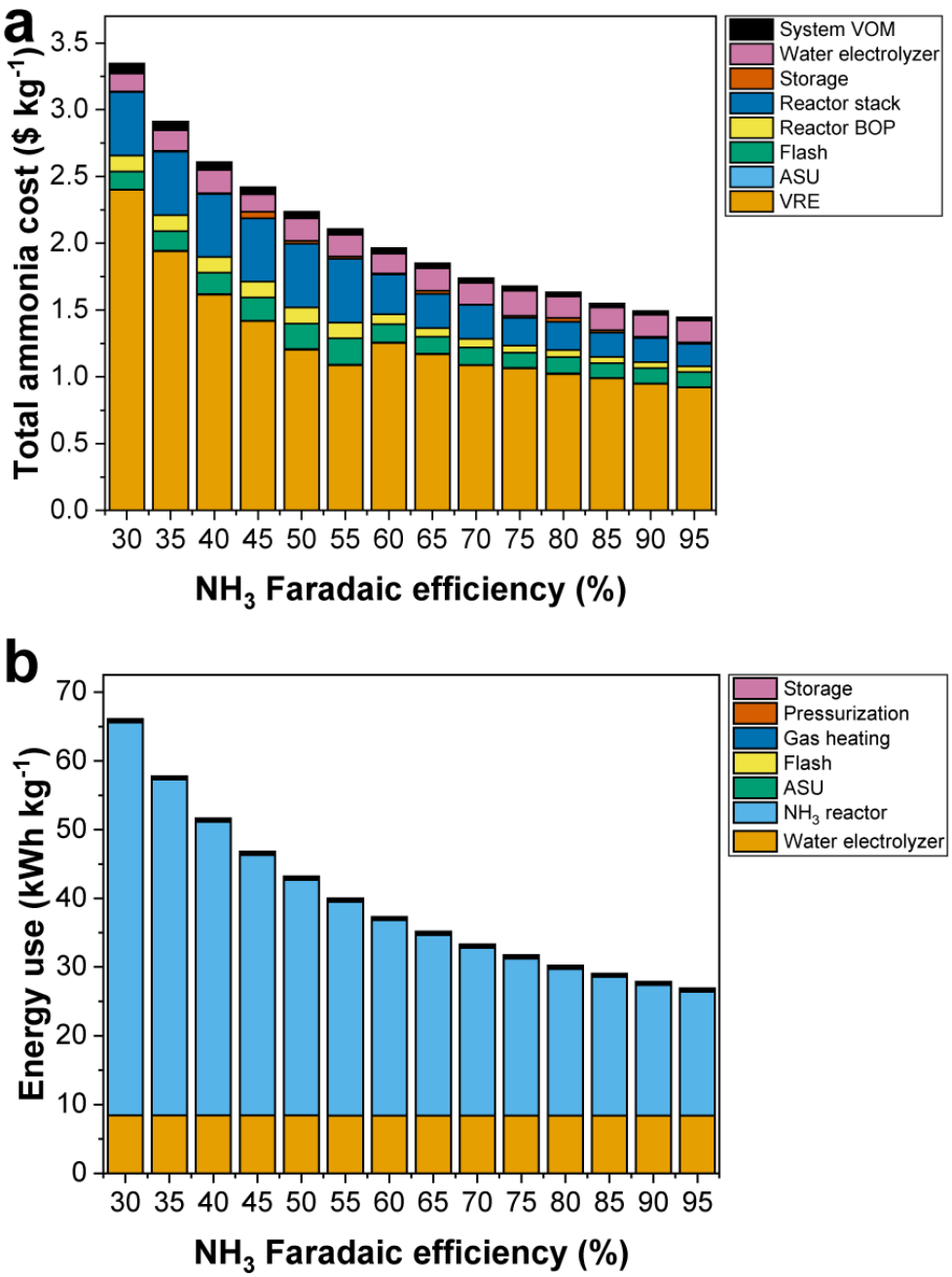

Fig. S7. The contributions of various parts of the ammonia plant on the price of ammonia as a function of reactor Faradaic efficiency for a reactor with low energy efficiency when PV and wind in West Texas as the power source. The kinetic overpotential was assumed to be ~3 V, which is comparable to the overpotential observed in lithium-mediated nitrogen reduction; the energy efficiency for the reaction is thus low. At low Faradaic efficiencies, both a larger reactor and more energy generation is necessary to produce the necessary amount of ammonia, thus increasing NH_3 costs significantly.

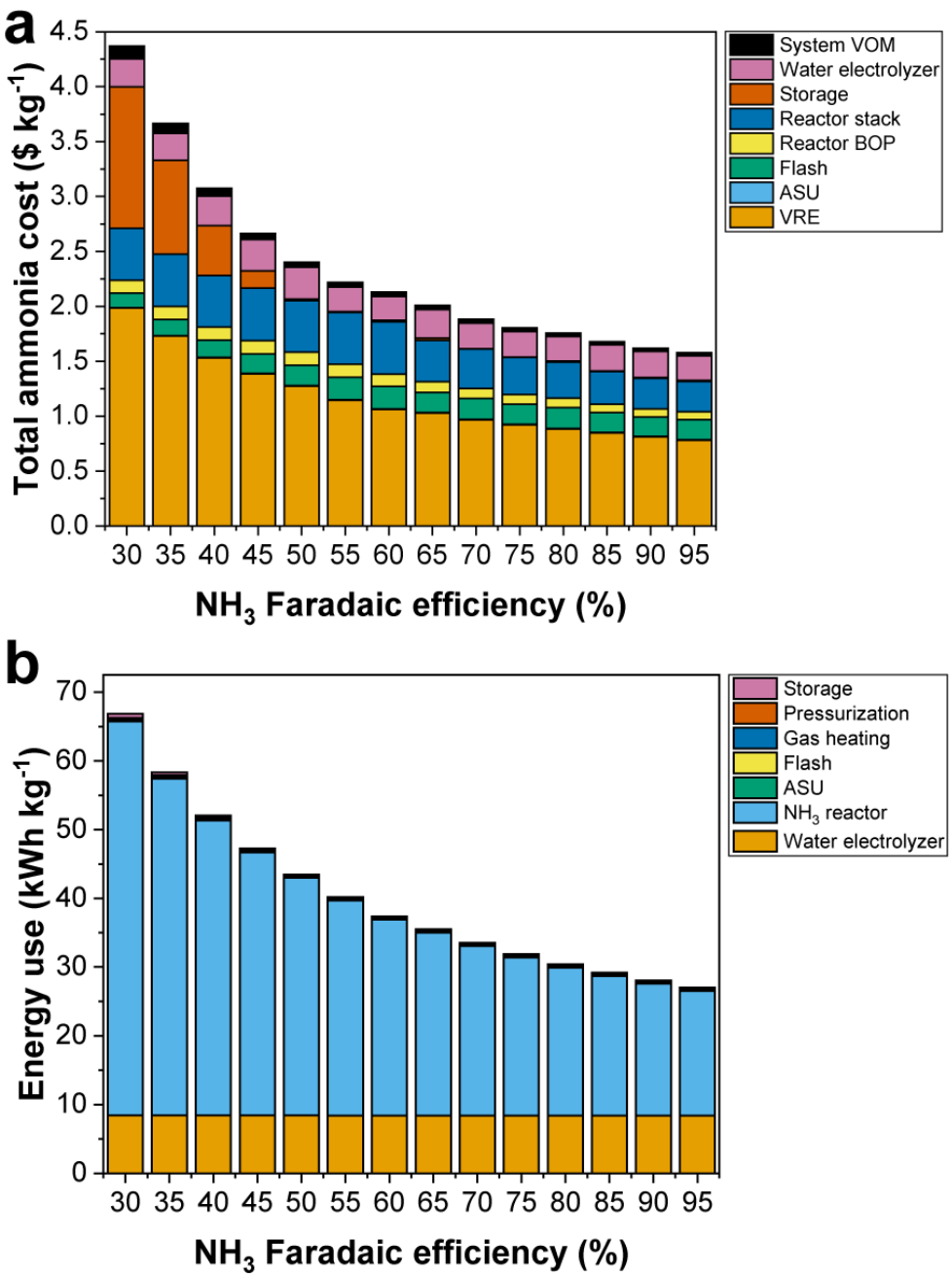

Fig. S8. The contributions of various parts of the ammonia plant on the price of ammonia as a function of reactor Faradaic efficiency for a reactor with low energy efficiency and only PV power. The kinetic overpotential was assumed to be ~3 V, which is comparable to the overpotential observed in lithium-mediated nitrogen reduction; the energy efficiency for the reaction is thus low. Only PV power was available to the model. At low Faradaic efficiencies, it is optimal to build energy storage (including expensive battery storage) and run ammonia production continuously instead of oversizing the plant to always operate at peak capacity. Due to the high cost of storage, NH3 is produced at high cost (but at a strictly lower cost than if storage were not used, by model design).

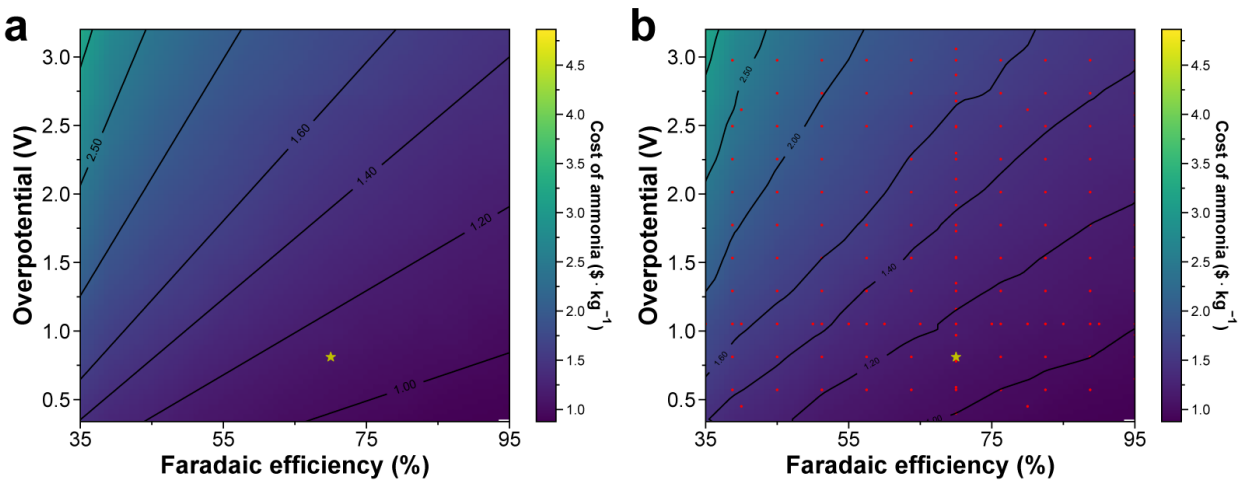

Fig. S9. Effect of Faradaic efficiency and cell overpotential on the cost of ammonia. (a) The data with smoothed contours. (b) The locations of data points used to generate the plots in red, and contours obtained by linear interpolation of values between points using SciPy griddata interpolation. The smoothed contours were obtained by fitting the data to a likely non-physical functional form that can accurately describe the data. The function used in (a) is $Cost = \frac{1006.8 \cdot \eta + 43.883 \cdot FE}{55.14 \cdot \eta + 60.64 \cdot FE - 790.9}$, where the cost is given in $ kg-1, FE is given in percentage units, and η is given in V units.

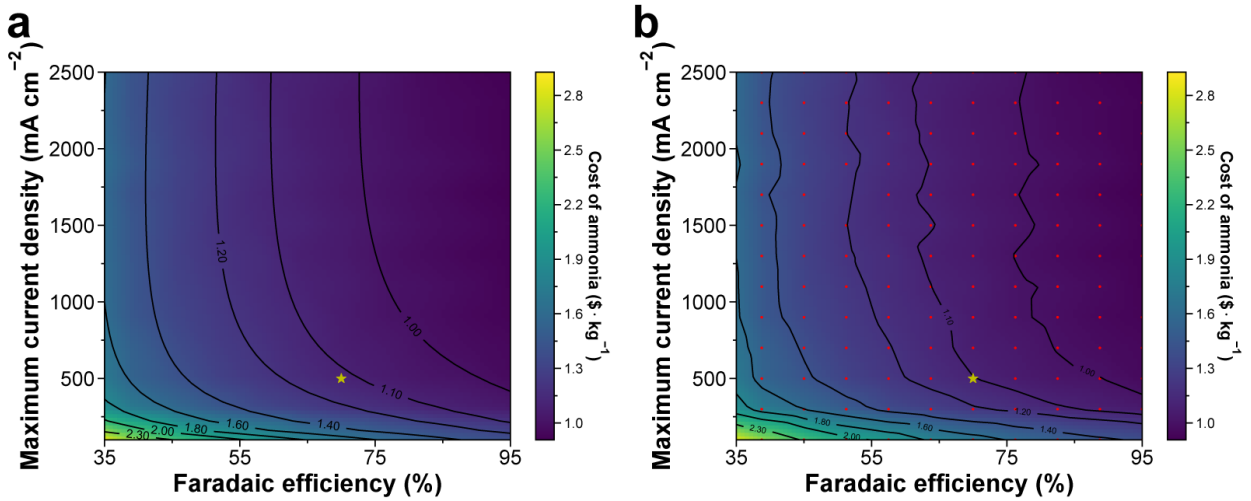

Fig. S10. Effect of Faradaic efficiency and maximum possible current density on the cost of ammonia. (a) The data with smoothed contours. (b) The locations of data points used to generate the plots in red, and contours obtained by linear interpolation of values between points using SciPy griddata interpolation. The smoothed contours were obtained by fitting the data to a likely non-physical functional form that can accurately describe the data. The function used in (a) is $Cost = 0.0037 \cdot FE + \frac{41.6303+0.09228 \cdot FE}{FE-0.001373 \cdot J_{max}} + \frac{831.755-6.4251 \cdot FE}{FE+4.41454 \cdot J_{max}}$, where the cost is given in $ kg-1, FE is given in percentage units, and J_{max} is given in mA cm-2 units.

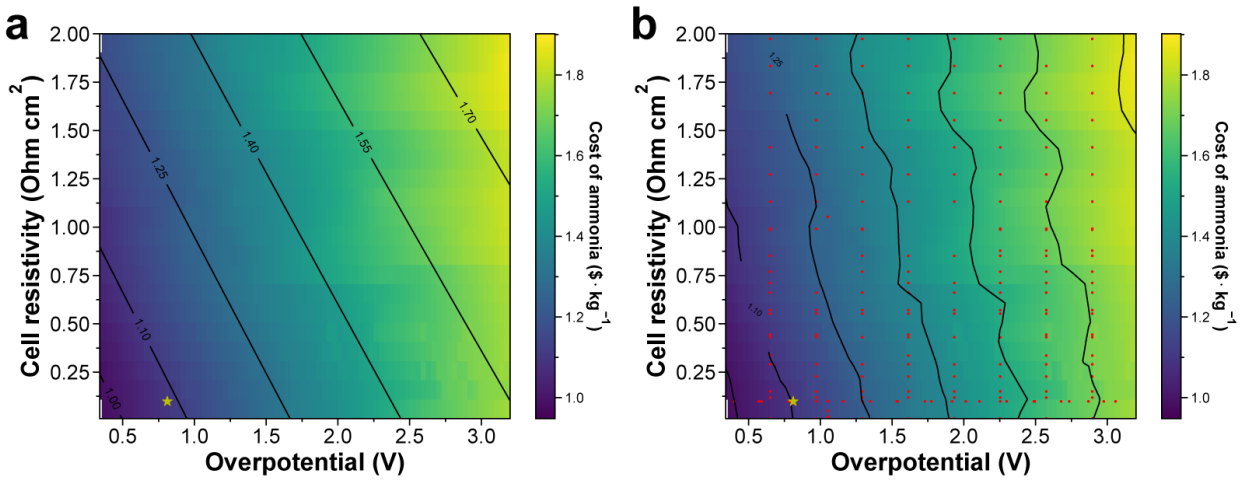

Fig. S11. Effect of cell overpotential and electrolyte resistivity on the cost of ammonia, with all parameters but the overpotential and electrolyte resistivity having base case values (Table 1). (a) The data with smoothed contours. (b) The locations of data points used to generate the plots in red, and contours obtained by linear interpolation of values between points using SciPy griddata interpolation. The smoothed contours were obtained by fitting the data to a potentially physical functional form that can accurately describe the data. The function used in (a) is $Cost = 0.075462 \cdot R + 0.265 \cdot \eta + 0.908$, where the cost is given in $ kg-1, R is given in Ohm cm2 units, and η is given in V units.

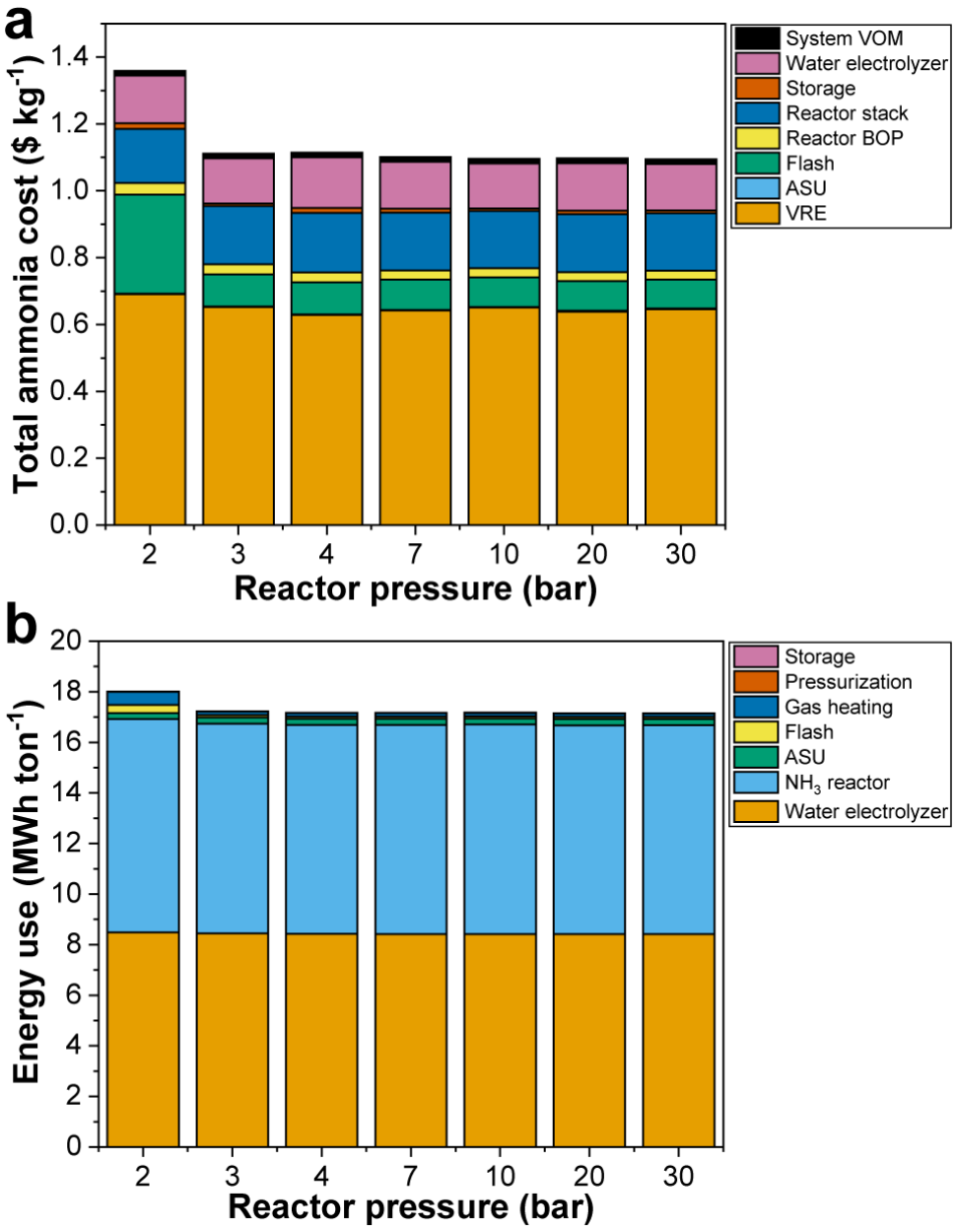

Fig. S12. Effect of the gas pressure in the plant (i.e. in the reactor, flash unit, and piping) on the cost of NH3. (a) The capital costs of individual components of the plant as a function of pressure. (b) Breakdown of the energy used to produce ammonia, which demonstrates what the VRE is used for. The pressure does not affect the cost of ammonia significantly above pressures of ~3 bar. Below this pressure, the flash unit cannot separate ammonia from the gas stream well, leading to an increase in several parts of the reactor. Note that the current model does not model the effect of pressure on reaction rates or increases in capital costs of equipment. It is likely that elevated pressures (>10 bar) would require higher-cost high-pressure equipment; there likely is an optimum operating pressure for an electrochemical ammonia synthesis reactor which balances out reaction rates, efficiency of separation, and costs of capital equipment.

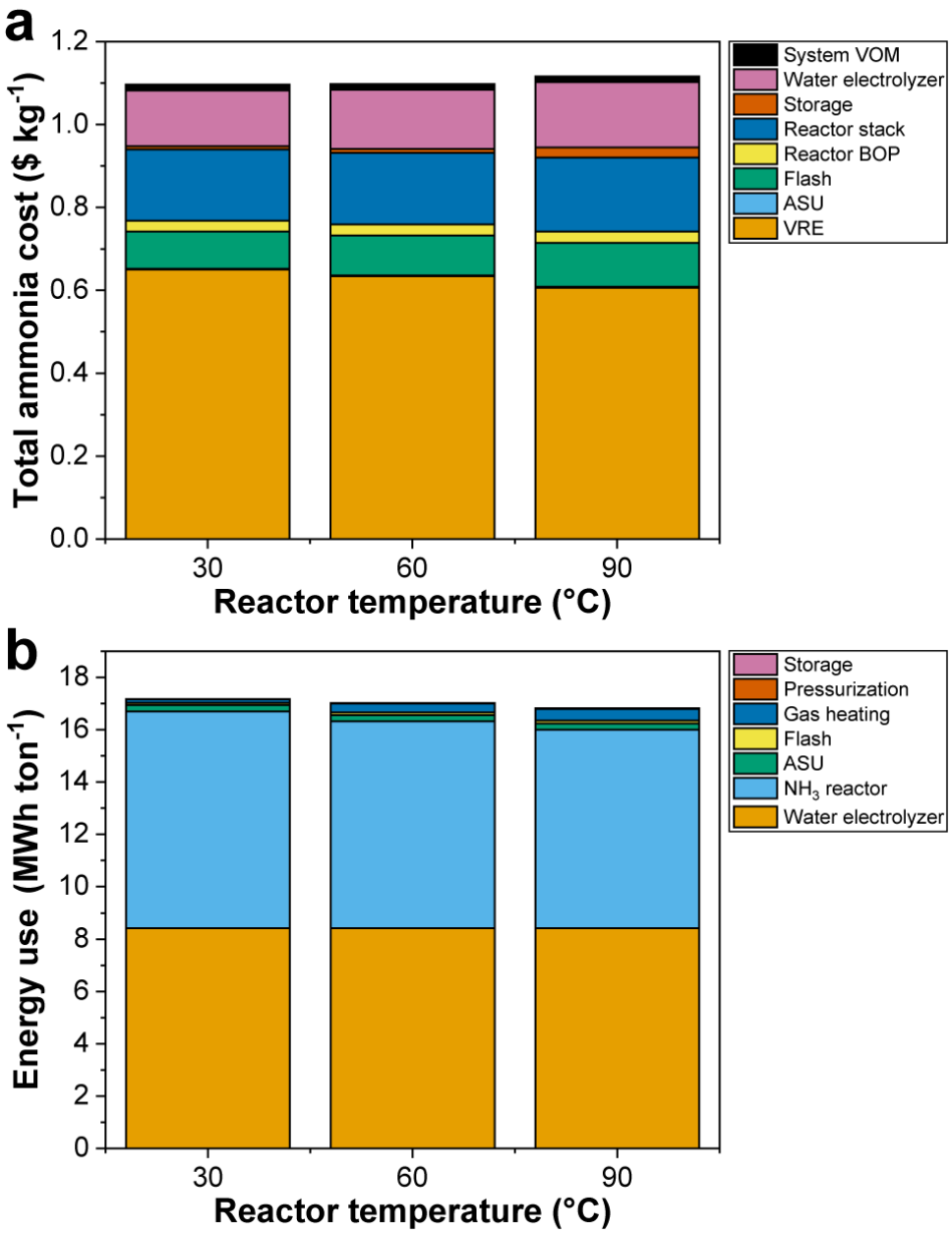

Fig. S13. Effect of the temperature of the electrochemical reactor on the cost of NH3. (a) The capital costs of individual components of the plant as a function of temperature. (b) Breakdown of the energy used to produce ammonia, which demonstrates what the VRE is used for. The reactor temperature does not significantly affect costs, though elevated temperatures decrease the energy consumption (VRE) and size of the reactor somewhat due to more efficient reactions.

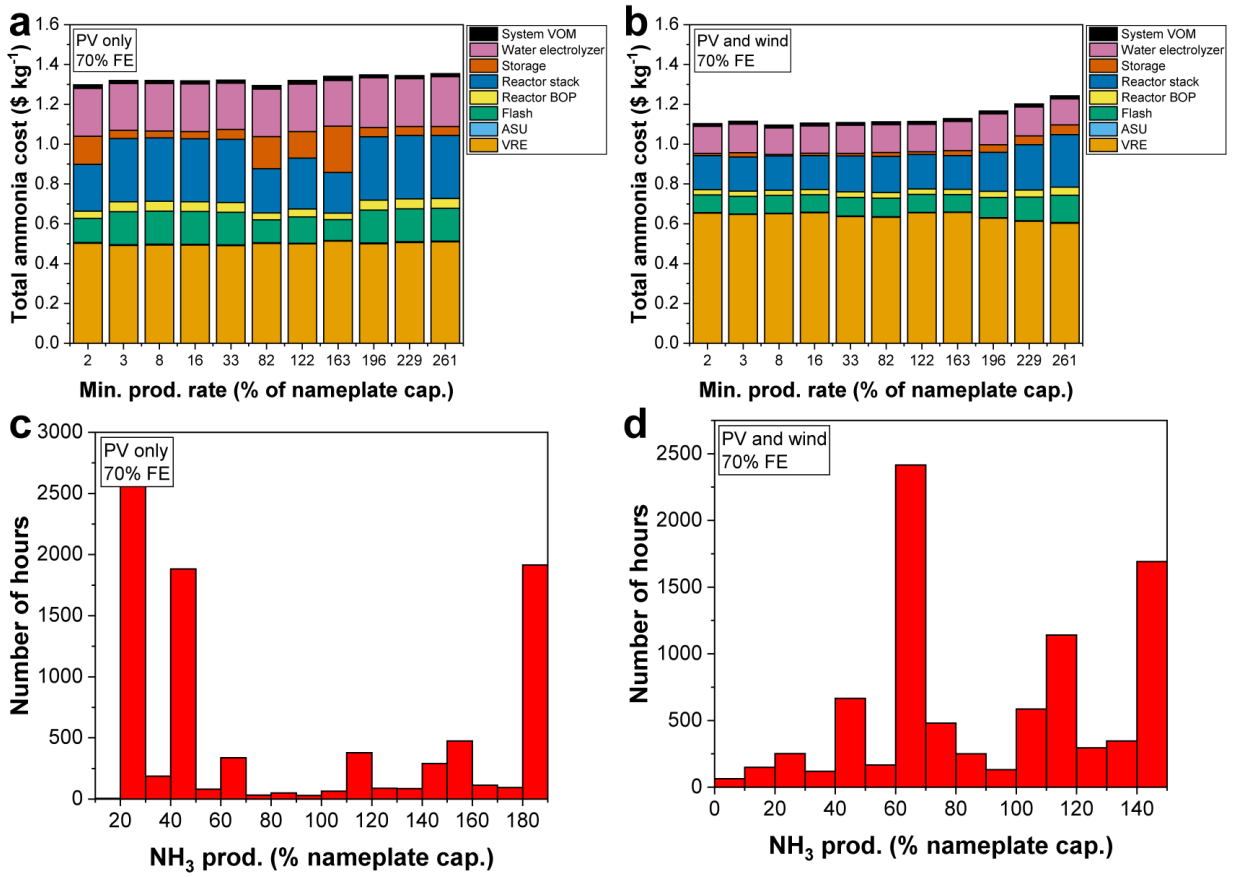

Fig. S14. Effect of the minimum necessary production rate on the cost of ammonia. (a, b) Effects of various minimum NH_3 production rates as a fraction of the nameplate capacity (250 ton/day) on the cost of ammonia when using (a) PV only or (b) PV and wind in West Texas as energy sources. In the case of PV-only, the costs are relatively unchanged with different minimum production rates, while they increase in the PV and wind case as the plant becomes less flexible. However, the cost of produced ammonia is lower in the PV and wind case when the plant is flexible. (c, d) The distributions of the production rates over a year with an 8% of nameplate capacity minimum production rate using the PV only and PV and wind cases, respectively.

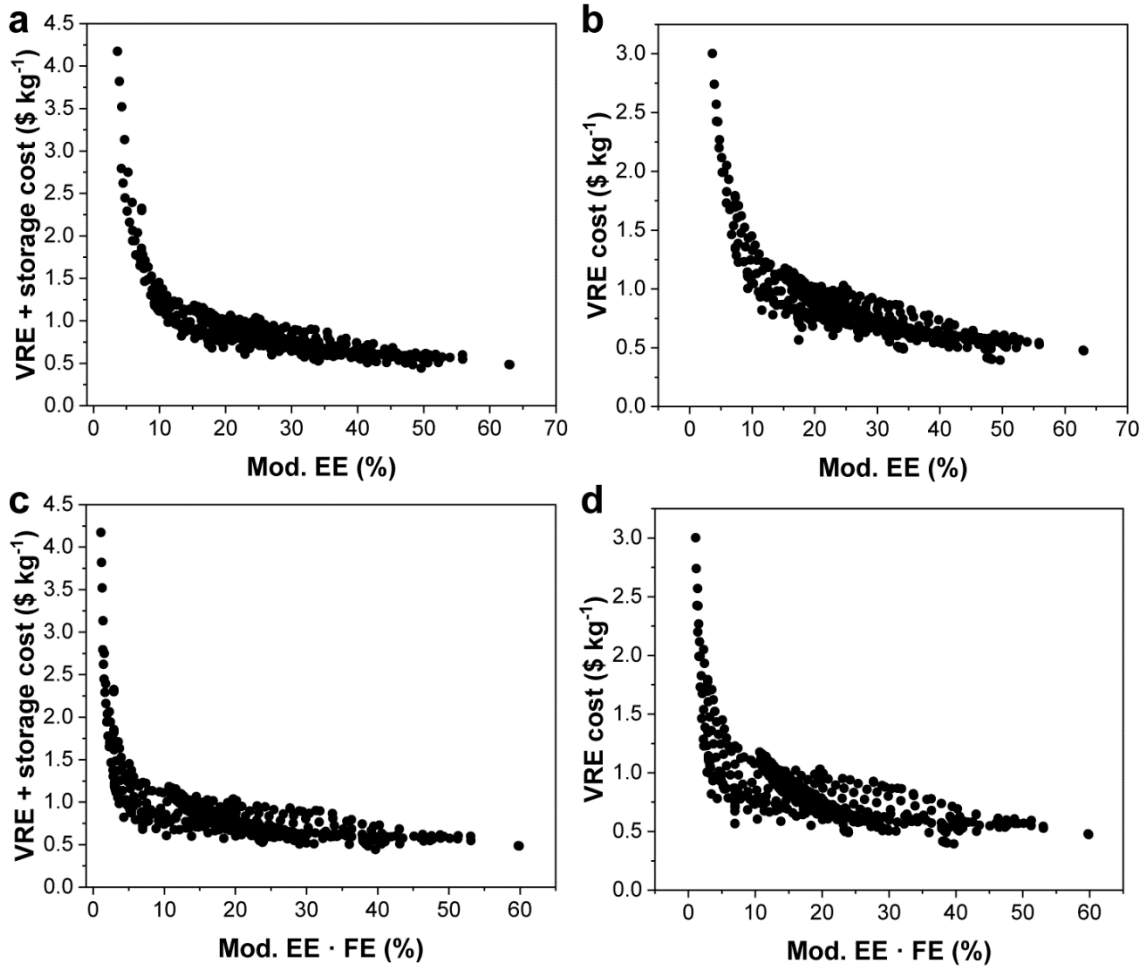

Fig. S15. The correlation between various energy efficiency groupings and the combined contribution of VRE generation and energy storage (energy cost for short) to ammonia cost (a). The correlation between the modified energy efficiency and energy cost. (b) The correlation between the modified energy efficiency and only VRE generation cost. (c) The correlation between the product of the modified energy efficiency and Faradaic efficiency and energy cost. (b) The correlation between the product of the modified energy efficiency and Faradaic efficiency and only VRE generation cost.

Supplementary References

37. F. Holmgren, W., W. Hansen, C. & A. Mikofski, M. Pvlib Python: a Python Package for Modeling Solar Energy Systems. *J. Open Source Softw.* **3**, 884 (2018).
38. Sengupta, M. *et al.* The National Solar Radiation Data Base (NSRDB). *Renew. Sustain. Energy Rev.* **89**, 51–60 (2018).
39. Draxl, C., Hodge, B.-M., Clifton, A. & Mccaa, J. Overview and Meteorological Validation of the Wind Integration National Dataset Toolkit. *NREL/TP-5000-61740. Golden Natl. Renew. Energy Lab. (forthcoming), Tech. Rep.* 87 (2015).
40. Mallapragada, D. S., Gencer, E., Insinger, P., Keith, D. W. & O'Sullivan, F. Can industrial-scale solar hydrogen supplied from commodity technologies be cost competitive by 2030? *Under Rev.* 1–38.
41. Proost, J. State-of-the art CAPEX data for water electrolysers, and their impact on renewable hydrogen price settings. *Int. J. Hydrogen Energy* **44**, 4406–4413 (2019).
42. Mayyas, A. *et al.* Manufacturing Cost Analysis for Proton Exchange Membrane Water Electrolyzers Manufacturing Cost Analysis for Proton Exchange Membrane Water Electrolyzers. (2019).
43. Lin, B., Wiesner, T. & Malmali, M. Performance of a Small-Scale Haber Process: A Techno-Economic Analysis. *ACS Sustain. Chem. Eng.* **8**, 15517–15531 (2020).
44. Akar, S. *et al.* 2020 Annual Technology Baseline (ATB) Cost and Performance Data for Electricity Generation Technologies. doi:10.7799/1644189.
45. Ahluwalia, R. K., Papadias, D. D., Peng, J.-K. & Roh, H. S. System Level Analysis of Hydrogen Storage Options (Project ID: ST-001). *U.S. DOE Hydrog. Fuel Cells Progr. 2019 Annu. Merit Rev. Peer Eval. Meet. - Washington, DC, 29 Apr - 1 May, 2019* (2019).
46. Kim, J., Noh, Y. & Chang, D. Storage system for distributed-energy generation using liquid air combined with liquefied natural gas. *Appl. Energy* **212**, 1417–1432 (2018).
47. Appl, M. Storage and Shipping. in *Ammonia* 213–220 (Wiley-VCH Verlag GmbH, 2007). doi:10.1002/9783527613885.ch09.
48. D'Ambrosio, C., Lodi, A. & Martello, S. Piecewise linear approximation of functions of two variables in MILP models. *Oper. Res. Lett.* **38**, 39–46 (2010).
49. Mallapragada, D. S., Sepulveda, N. A. & Jenkins, J. D. Long-run system value of battery energy storage in future grids with increasing wind and solar generation. *Appl. Energy* **275**, 115390 (2020).
50. Gurobi Optimization, LLC. Gurobi Optimizer Reference Manual. (2022).
51. Reuther, A. *et al.* Interactive supercomputing on 40,000 cores for machine learning and data analysis. in *2018 IEEE High Performance extreme Computing Conference (HPEC)* 1–6 (2018).
52. Suryanto, B. H. R., Wang, Y., Hocking, R. K., Adamson, W. & Zhao, C. Overall electrochemical splitting of water at the heterogeneous interface of nickel and iron oxide. *Nat. Commun.* **10**, 1–10 (2019).
53. Blanford, G. J., Merrick, J. H., Bistline, J. E. T. & Young, D. T. Simulating Annual Variation in Load, Wind, and Solar by Representative Hour Selection. *Energy J.* **39**, 189–212 (2018).
54. G. J. Suppes; Walas, S. M. Heuristics in Chemical Engineering. *Chem. Process Equip. Sel. Des.* (2002).
55. Garland, M. & Heckbert, P. S. Surface simplification using quadric error metrics. *Proc.*

24th Annu. Conf. Comput. Graph. Interact. Tech. SIGGRAPH 1997 209–216 (1997) doi:10.1145/258734.258849.
56. Magnusson, J. Quadratic Mesh Simplification. (2020).
57. Avramov, S. G., Lefterova, E., Penchev, H., Sinigersky, V. & Slavcheva, E. Comparative study on the proton conductivity of perfluorosulfonic and polybenzimidazole based polymer electrolyte membranes. *Bulg. Chem. Commun.* **48**, 43–50 (2016).
58. Slade, S., Campbell, S. A., Ralph, T. R. & Walsh, F. C. Ionic Conductivity of an Extruded Nafion 1100 EW Series of Membranes. *J. Electrochem. Soc.* **149**, A1556 (2002).
59. Tsuneto, A., Kudo, A. & Sakata, T. Lithium-mediated electrochemical reduction of high pressure N_2 to NH_3. *J. Electroanal. Chem.* **367**, 183–188 (1994).
60. Sánchez, A. & Martín, M. Scale up and scale down issues of renewable ammonia plants: Towards modular design. *Sustain. Prod. Consum.* **16**, 176–192 (2018).
61. Hu, T., Zhou, H., Peng, H. & Jiang, H. Nitrogen production by efficiently removing oxygen from air using a perovskite hollow-fiber membrane with porous catalytic layer. *Front. Chem.* **6**, 1–7 (2018).
62. Martín, A. J. & Pérez-Ramírez, J. Heading to Distributed Electrocatalytic Conversion of Small Abundant Molecules into Fuels, Chemicals, and Fertilizers. *Joule* **3**, 2602–2621 (2019).
63. Schmidt, O. *et al.* Future cost and performance of water electrolysis: An expert elicitation study. *Int. J. Hydrogen Energy* **42**, 30470–30492 (2017).
64. Li, S., Medrano, J. A., Hessel, V. & Gallucci, F. Recent progress of plasma-assisted nitrogen fixation research: A review. *Processes* **6**, (2018).
65. Rouwenhorst, K. H. R. *et al.* Plasma-driven catalysis: Green ammonia synthesis with intermittent electricity. *Green Chem.* **22**, 6258–6287 (2020).
66. Schiffer, Z. J. & Manthiram, K. Electrification and Decarbonization of the Chemical Industry. *Joule* **1**, 10–14 (2017).
67. Smith, C., McCormick, A. V. & Cussler, E. L. Optimizing the Conditions for Ammonia Production Using Absorption. *ACS Sustain. Chem. Eng.* **7**, 4019–4029 (2019).
68. Li, K. *et al.* Increasing Current Density of Li-Mediated Ammonia Synthesis with High Surface Area Copper Electrodes. *ACS Energy Lett.* **7**, 36–41 (2022).
69. Brauns, J. & Turek, T. Experimental evaluation of dynamic operating concepts for alkaline water electrolyzers powered by renewable energy. *Electrochim. Acta* **404**, 139715 (2022).